JOURNAL OF GEOPHYSICAL RESEARCH, VOL. 111, E12S11, doi:10.1029/2006JE002797, 2006

Nickel on Mars: Constraints on meteoritic material at the surface

A. S. Yen,[1] D. W. Mittlefehldt,[2] S. M. McLennan,[3] R. Gellert,[4] J. F. Bell III,[5] H. Y. McSween Jr.,[6] D. W. Ming,[2] T. J. McCoy,[7] R. V. Morris,[2] M. Golombek,[1] T. Economou,[8] M. B. Madsen,[9] T. Wdowiak,[10] B. C. Clark,[11] B. L. Jolliff,[12] C. Schröder,[13] J. Brückner,[14] J. Zipfel,[15] and S. W. Squyres[5]

Received 20 July 2006; revised 28 September 2006; accepted 6 November 2006; published 15 December 2006.

[1] Impact craters and the discovery of meteorites on Mars indicate clearly that there is meteoritic material at the Martian surface. The Alpha Particle X-ray Spectrometers (APXS) on board the Mars Exploration Rovers measure the elemental chemistry of Martian samples, enabling an assessment of the magnitude of the meteoritic contribution. Nickel, an element that is greatly enhanced in meteoritic material relative to samples of the Martian crust, is directly detected by the APXS and is observed to be geochemically mobile at the Martian surface. Correlations between nickel and other measured elements are used to constrain the quantity of meteoritic material present in Martian soil and sedimentary rock samples. Results indicate that analyzed soils samples and certain sedimentary rocks contain an average of 1% to 3% contamination from meteoritic debris.

Citation: Yen, A. S., et al. (2006), Nickel on Mars: Constraints on meteoritic material at the surface, *J. Geophys. Res.*, *111*, E12S11, doi:10.1029/2006JE002797.

1. Introduction

[2] In the ongoing study of the composition, origin, and weathering of rocks and soils at the surface of Mars, it is essential to understand the magnitude of meteoritic contributions. Analyses of minor and trace elements establish the geochemical history of surface materials, and neglecting to account for signatures of material non-native to Mars may result in erroneous interpretations. Quantifying the meteoritic influx of organic material is vital for constraining carbon oxidation rates in support of Martian habitability assessments, and establishing the likelihood that future sample return missions will collect meteoritic rather than Martian material is essential in developing mission strategies. In addition, the quantity of meteoritic material in the soils establishes age constraints, with potentially important implications for the geological and climatic history of the surface.

[3] In lunar soils, the meteoritic component is established to be 1.5–2% with a composition consistent with the CI class of carbonaceous chondrites [*Taylor*, 1982]. Given its size, its location, and presence of an atmosphere, the preservation of meteoritic material at the surface of Mars could be substantially higher [*Boslough*, 1988, 1991]. Estimates of the fine-grained meteoritic contribution to the Martian surface in previous studies, however, vary widely. Extrapolating from accumulation rates measured at Earth, *Flynn and McKay* [1990] estimate that the Martian soil contains between 2% and 29% meteoritic matter by mass. *Morris et al.* [2000] tested a variety of mixing models to explain Pathfinder soils and found that the compositions were consistent with 0%–22% meteoritic material. Comparing Martian meteorite analyses with Viking Lander data, *Newsom and Hagerty* [1997] suggested that up to 10% of the iron in Martian soils could be meteoritic, corresponding to an overall meteoritic concentration of up to 7%. *Yen and Murray* [1998] describe a model predicting a total accumulated nickel abundance in excess of 1000 ppm, equivalent to approximately 7.5% meteoritic material at the Martian surface. On the basis of Viking analyses, *Clark and Baird* [1979] showed that up to 40% meteoritic material could be consistent with the elemental chemistry of the analyzed soil samples. It is clear that there have been significant uncer-

[1] Jet Propulsion Laboratory, California Institute of Technology, Pasadena, California, USA.
[2] NASA Johnson Space Center, Houston, Texas, USA.
[3] Department of Geosciences, State University of New York at Stony Brook, Stony Brook, New York, USA.
[4] Department of Physics, University of Guelph, Guelph, Ontario, Canada.
[5] Department of Astronomy, Cornell University, Ithaca, New York, USA.
[6] Department of Earth and Planetary Sciences, University of Tennessee, Knoxville, Tennessee, USA.
[7] National Museum of Natural History, Smithsonian Institution, Washington, D.C., USA.
[8] Enrico Fermi Institute, University of Chicago, Chicago, Illinois, USA.
[9] Niels Bohr Institute, University of Copenhagen, Copenhagen, Denmark.
[10] Department of Physics, University of Alabama at Birmingham, Birmingham, Alabama, USA.
[11] Lockheed Martin Corporation, Littleton, Colorado, USA.
[12] Department of Earth and Planetary Sciences, Washington University, St. Louis, Missouri, USA.
[13] Johannes Gutenberg University, Mainz, Germany.
[14] Max Planck Institut für Chemie, Mainz, Germany.
[15] Forschungsinstitut und Naturmuseum Senckenberg, Frankfurt, Germany.

0148-0227/06/2006JE002797$09.00

tainties in the accumulations of meteoritic material in the Martian surface layer.

[4] The Mars Exploration Rovers (MER) provide a new and unique capability for addressing the magnitude of the meteoritic contributions to the Martian surface. The instrument suite on board each rover consists of a 0.27 mrad/pixel, multiple filter Panoramic camera [*Bell et al.*, 2003], a miniature Thermal Emission Spectrometer covering the 5 to 29 μm wavelength region [*Christensen et al.*, 2003], a 30 μm/pixel Microscopic Imager [*Herkenhoff et al.*, 2003], an Alpha Particle X-ray Spectrometer (APXS) for elemental composition [*Rieder et al.*, 2003], a Mössbauer Spectrometer for mineralogy of iron-bearing phases [*Klingelhöfer et al.*, 2003], a set of magnets for attracting dust particles [*Madsen et al.*, 2003], a Rock Abrasion Tool (RAT) to remove surface contamination and weathering rinds from rock surfaces [*Gorevan et al.*, 2003], and engineering cameras to support mobility, navigation, science, and placement of the instrument arm [*Maki et al.*, 2003].

[5] In this paper, we show how the MER instruments in combination with the mobility of the rovers have been used to evaluate the quantity of fine-grained meteoritic materials dispersed in the surficial deposits and ancient sedimentary rocks encountered at Gusev crater by Spirit and by Opportunity on the Meridiani plains. The initial form of this material may have been interplanetary dust particles, micrometeorites, or comminuted, vaporized and/or recondensed portions of larger objects.

[6] In section 2 we examine evidence for meteors and meteorites from MER imaging data sets to illustrate a clear exogenic contribution to the Martian surface. In section 3 we show that MER APXS measurements of nickel content provide the primary constraints on the magnitude of a possible meteoritic contribution to the samples analyzed at both rover sites. We then examine the observed concentrations of nickel in section 4, and assess possible mixing relationships between a meteoritic component and Martian materials in section 5. Quantitative constraints on the meteoritic infall are presented in section 6. Relationships to the magnetic properties investigations of Martian soil and dust are described in section 7. In section 8, meteoritic infall estimates derived from nickel measurements are compared to models of likely meteoritic contribution based on observed impact craters and the influx of interplanetary dust particles. In section 9, we synthesize these different measurements and approaches to arrive at an estimate of the minimum and maximum likely magnitude of the meteoritic component of the Martian surface. Finally, in section 10, implications for the meteoritic carbon abundance at the Martian surface are presented.

2. Meteors and Meteorites

[7] MER observations and measurements provide clear macroscopic evidence for a meteoritic contribution to the Martian surface. Abundant impact craters, hollows, shallow depressions, and small pits (Figure 1) are all evidence of material falling from above. Many of the smaller craters observed directly by MER may be the result of secondary impacts but nevertheless provide unambiguous evidence that the surface of Mars has been profoundly influenced by meteorite impact.

[8] One serendipitous observation provides remarkable evidence for ongoing influx of meteoritic material to the Martian surface. A Pancam image collected by Spirit on sol 63 shows a streak with an orientation, apparent velocity, and light curve consistent with a meteor originating from dust shed along a cometary orbit [*Selsis et al.*, 2005]. A number of other studies have also pointed out the likelihood of Martian meteor detection and the probability of the resulting delivery of meteoritic fragments to the surface [e.g., *Davis*, 1993; *Adolfsson et al.*, 1996; *Christou and Beurle*, 1999].

[9] Over a traverse of 8.5 kilometers, Opportunity has analyzed two meteorites, and has perhaps driven past many more, on the surface of Meridiani Planum. A ~30 cm diameter rock in the plains south of Endurance crater known informally as "Heatshield Rock" (Figure 2) was determined by the Mössbauer spectrometer to have ~94% of its iron in the iron-nickel alloy kamacite [*Morris et al.*, 2006b] and by the APXS to have a total of 7 wt% Ni (R. Gellert et al., In situ chemistry along the traverse of Opportunity at Meridiani Planum: Sulfate rich outcrops, iron rich spherules, global soils and various erratics, manuscript in preparation, 2006; hereinafter referred to as Gellert et al., manuscript in preparation, 2006). This rock is a meteorite on the surface of Mars and has been classified as a IAB iron formally designated "Meridiani Planum" by the Meteoritical Society nomenclature committee.

[10] A small (~3 cm diameter) rock fragment (informally referred to as "Barberton", Figure 3) analyzed by the Opportunity APXS and Mössbauer spectrometers at the rim of Endurance crater was originally thought to be an olivine-rich basaltic pebble ejected from some other locality on Mars. Upon closer examination of the data, this pebble was found to exhibit a weak magnetic sextet in the Mössbauer data consistent with iron in the form of kamacite, which does not occur in Martian basalts [*Morris et al.*, 2006b]. This observation in combination with one of the highest Ni concentrations measured on Mars (~1700 ppm) indicates that this pebble is not a piece of Mars. The elemental composition of this sample, but perhaps not the mineralogy, is most consistent with a mesosiderite [*Schröder et al.*, 2006]. Barberton could be a fragment of a larger impactor or a member of the population 20 to 50 gram objects predicted to survive intact to the Martian surface [*Bland*, 2001].

[11] Given the abundance of rocks at the Gusev landing site relative to the Meridiani plains, meteorites are more difficult to find. Nonetheless, the Spirit Mini-TES has identified two ~25 to 30 cm rocks with thermal infrared characteristics similar to those of Heatshield Rock (S. Ruff, personal communications, 2006).

[12] There is clearly direct evidence for a rare but "macroscopic" meteoritic population at the surface of Mars. A more challenging issue is determining the magnitude of the "microscopic" meteoritic component of the Martian surface. That is, what is the fraction of the soil or of sedimentary rocks that is meteoritic? Answering this question requires a more detailed assessment of the chemistry of fine-grained materials on the surface, with a specific

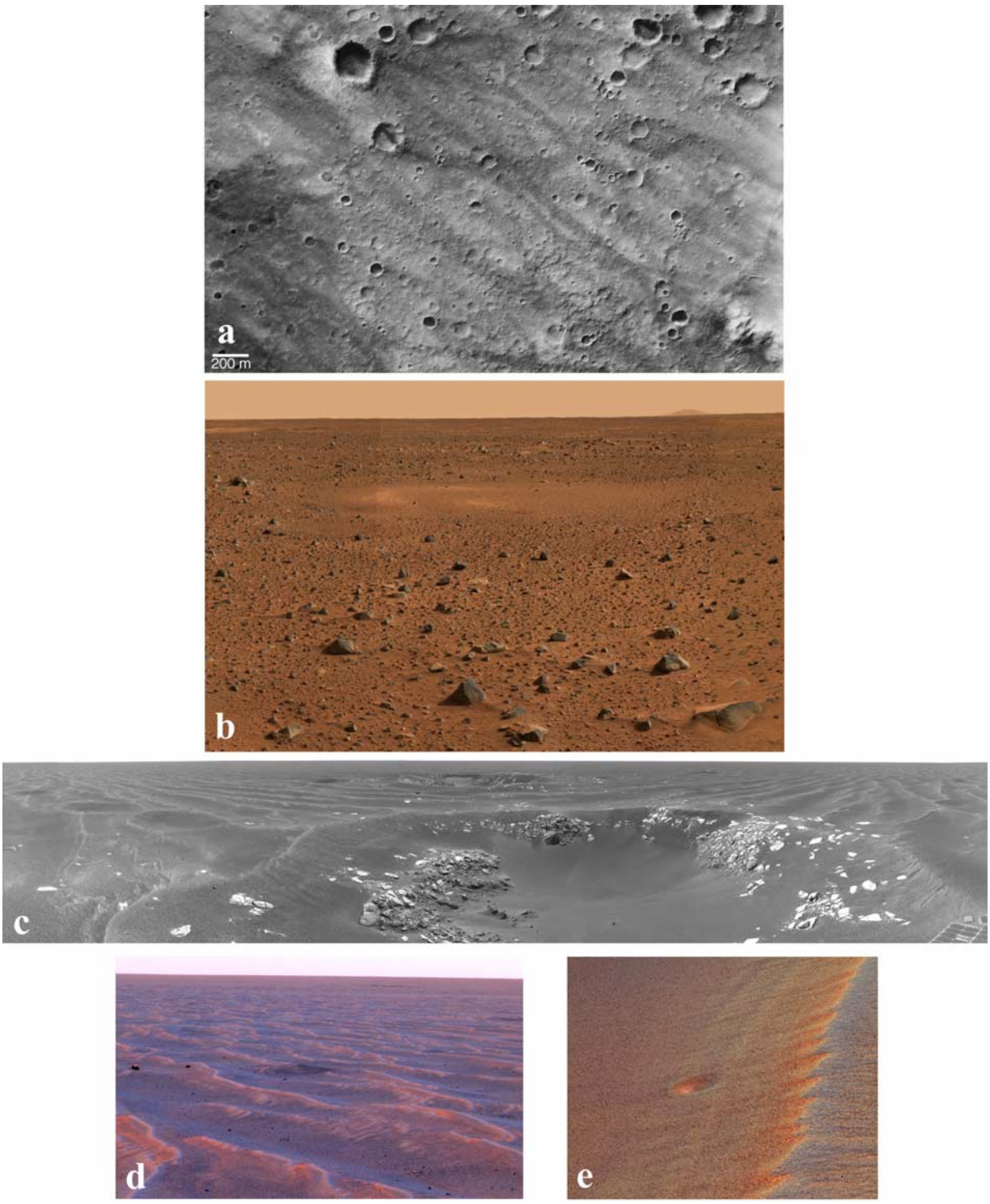

Figure 1. Indications of meteoritic input to the Martian surface: (a) Mars Orbiter Camera image showing the cratered surface of the Gusev plains [*Malin et al.*, 2005]. The Spirit rover track traverse extends from the lander to Bonneville crater (upper left) to the West Spur of the Columbia Hills (lower right). (b) A rock-deficient "hollow" is apparent after an impact crater is filled with aeolian sediments (a portion of the Spirit "Mission Success" Pan). (c) Navcam image of small impact craters (possibly secondaries) at Meridiani Planum (sol 387). The diameter of the crater in the foreground is approximately 8 meters. (d) False color Pancam image of an impact depression (center of image), possibly due to ejecta, with associated debris which postdates aeolian bedforms (Opportunity sol 373, sequence p2375). (e) False color Pancam image of a ~20 cm diameter pit in the Meridiani sand sheet (sol 436, sequence p2592), consistent with models of centimeter-scale objects impacting the surface [*Hörz et al.*, 1999].

Figure 2. Approximate true color Pancam image of an iron-nickel meteorite found near the Opportunity heat shield designated "Meridiani Planum" by the Meteoritical Society nomenclature committee (sol 346, sequence p2591).

focus on key elements that can be tracers of a meteoritic contribution.

3. Elemental Tracers

[13] The Alpha Particle X-ray Spectrometers (APXS) utilizes a combination of Particle Induced X-ray Emission (PIXE) and X-ray Fluorescence (XRF) spectroscopic techniques to determine the elemental composition of analyzed samples [*Rieder et al.*, 2003]. Through sol 720, over 200 distinct targets have been analyzed at Gusev crater and Meridiani Planum. The following elements are typically measured in soil and rock samples at the two landings sites: Na, Mg, Al, Si, P, S, Cl, K, Ca, Ti, Cr, Mn, Fe, Ni, Zn, and Br [e.g., *Gellert et al.*, 2004]. Definitive detections of Co, Cu, Ga, Ge, Rb, Sr, Y, Ba, and Pb have also been made in certain specific samples [*Gellert et al.*, 2006; B. C. Clark et al., Evidence for montmorillonite or its compositional precursors in Columbia Hills, Mars, submitted to *Journal of Geophysical Research*, 2006 (hereinafter referred to as Clark et al., submitted manuscript, 2006)]. The APXS data which support the analyses in this paper are listed in Tables 1a and 1b.

3.1. Chondritic Nickel

[14] Of the 16 elements that are detected on a regular basis, nickel is the most effective for constraining the extent of meteoritic contributions to the Martian samples (Figure 4). Other elements, such as Fe, Mg, S, and Cr, even though they are typically enhanced in meteoritic material, are less useful in studying the exogenic contribution, as the range of Martian sample compositions encompasses the meteoritic abundances of these elements. That is, some samples analyzed by MER have greater concentrations of these elements, while others have less. This produces inherent difficulties in attempting to discern small admixtures of meteoritic elements other than nickel in the midst of significant diversity in rock and soil compositions.

[15] Ni is present in CI chondrites, representative of average solar system composition, at a level of 10.6 mg/g (13.1 mg/g on a volatile free basis) [*Lodders*, 2003]. This is roughly a factor of 20 larger than rocks analyzed by Opportunity, a factor of 90 times the concentration in Adirondack class basalts analyzed by Spirit, and between 30 and 410 times the Ni concentration typical of Martian meteorites [*Lodders*, 1998]. Other classes of chondrites that could potentially dominate the meteoritic material arriving at Mars all have high nickel. The H, L, and LL groups of ordinary chondrites, which dominate the observed falls on Earth, have average Ni concentrations of 17.1 mg/g, 12.4 mg/g, and 10.6 mg/g, respectively [*Lodders and Fegley*, 1998].

3.2. Other Elements

[16] The viability of using other potentially detectable trace elements in constraining the magnitude of meteoritic input to surface materials was assessed. Of the elements detectable by the MER APXS (X-ray energies between 1 and 16 keV) and not including the 16 elements that are typically quantifiable, cobalt is the most abundant in CI averages: 500 μg/g [*Lodders*, 2003]. Unfortunately, the separation between the Kα peak of Co at 6.93 keV and the Kβ peak of Fe at 7.06 keV is only 130 eV. Using a sensor with an inherent energy resolution of 170 eV under the best conditions means that these peaks are essentially superimposed. As a result, the quantity of Co required in a MER analysis to produce a confident detection is approximately 100 μg/g. This is 20% of the chondritic value and is

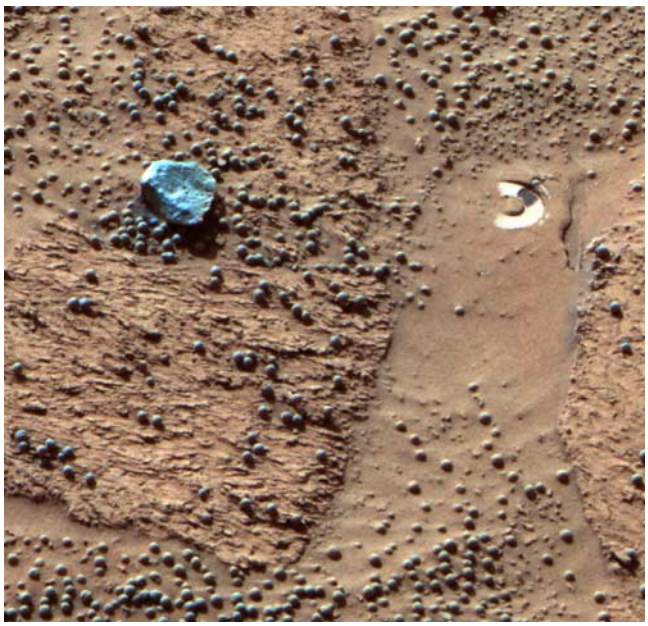

Figure 3. False color Pancam image from the rim of Endurance crater (sol 123, sequence p2535) of a likely meteorite fragment informally referred to as "Barberton." The backward "C" to the right of the rock fragment is an indentation made by the contact plate of the Mössbauer spectrometer.

Table 1a. APXS Data Used in This Paper[a]

Sample	Na_2O	MgO	Al_2O_3	SiO_2	P_2O_5	SO_3	Cl	K_2O	CaO	TiO_2	Cr_2O_3	MnO	FeO	Ni	Zn	Br
Gusev Basaltic Soils[b]																
A014	2.76	8.34	9.89	46.3	0.87	6.61	0.78	0.48	6.36	0.86	0.31	0.33	16.0	556	293	31
A041	2.80	8.67	10.02	46.0	0.80	5.26	0.69	0.43	6.98	0.72	0.49	0.36	16.6	341	329	112
A043	2.88	8.45	10.30	46.8	0.81	5.00	0.60	0.45	6.52	0.91	0.41	0.36	16.5	364	257	56
A044	2.54	8.69	10.23	46.3	0.87	6.06	0.71	0.43	6.58	0.77	0.26	0.29	16.2	287	246	38
A045	3.09	8.59	9.96	45.5	0.78	6.19	0.78	0.48	6.69	0.68	0.38	0.30	16.5	551	211	69
A047	3.13	8.41	10.05	46.0	0.86	6.33	0.73	0.44	6.32	0.89	0.33	0.34	16.1	318	288	19
A049	2.44	8.90	9.83	46.2	0.68	6.11	0.69	0.38	6.14	1.00	0.43	0.34	16.8	443	318	61
A050	2.65	8.77	9.96	46.1	0.73	5.69	0.77	0.37	6.24	1.02	0.40	0.35	16.8	592	255	65
A052	3.18	8.47	9.67	45.6	0.83	6.10	0.80	0.41	6.60	0.81	0.37	0.34	16.7	429	229	63
A065	3.20	8.57	9.86	45.9	0.81	6.76	0.84	0.47	6.04	0.83	0.31	0.31	15.9	620	435	0
A071	2.91	8.25	9.56	45.0	0.91	7.61	0.88	0.49	6.17	0.89	0.31	0.31	16.5	641	409	30
A074A	2.89	8.86	10.12	46.7	0.66	4.39	0.54	0.40	6.57	0.94	0.46	0.36	17.0	475	210	53
A074B	2.23	9.06	9.54	46.0	0.15	6.56	0.85	0.40	6.57	0.88	0.44	0.31	16.9	450	391	108
A105	3.01	8.43	9.68	46.3	0.79	6.67	0.72	0.44	6.45	0.89	0.32	0.34	15.8	237	308	11
A113	3.10	8.39	9.92	46.1	0.88	6.37	0.79	0.47	6.07	1.00	0.37	0.31	16.1	467	192	32
A122	3.07	8.41	10.65	47.0	0.95	5.45	0.63	0.47	6.38	0.88	0.33	0.28	15.4	391	239	31
A126	3.06	8.15	10.02	46.3	0.83	6.40	0.77	0.45	6.50	0.96	0.29	0.32	15.9	641	402	0
A135	3.04	8.73	10.71	47.0	0.77	4.67	0.54	0.42	6.27	0.89	0.42	0.34	16.1	483	291	19
A158	3.25	8.73	11.29	47.8	0.75	4.10	0.52	0.45	6.31	0.67	0.36	0.33	15.3	536	200	36
A227	2.77	8.42	9.59	45.7	0.87	7.50	0.94	0.49	5.88	0.84	0.28	0.31	16.3	533	264	263
A259	3.21	8.42	10.13	46.4	0.90	6.65	0.76	0.46	6.22	0.84	0.29	0.30	15.3	467	293	24
A280	3.17	8.94	9.80	45.0	1.02	6.48	0.87	0.42	6.36	0.88	0.34	0.34	16.2	469	252	101
A315	3.37	8.68	10.31	46.9	0.88	5.82	0.68	0.43	6.24	0.84	0.31	0.32	15.1	412	237	13
A342	3.45	9.42	10.63	46.7	0.84	4.80	0.57	0.40	6.20	0.70	0.33	0.31	15.5	679	162	37
A477	3.09	8.58	10.78	47.7	0.83	4.75	0.55	0.43	6.37	0.83	0.34	0.33	15.3	427	228	32
A587	3.18	8.61	9.79	45.4	0.93	7.42	0.83	0.45	6.08	0.86	0.26	0.31	15.7	433	411	31
A588	3.17	8.84	9.86	45.6	0.93	6.95	0.76	0.43	6.10	0.87	0.28	0.31	15.8	460	367	48
A607	3.48	8.13	11.38	47.0	1.11	5.28	0.60	0.46	6.33	1.17	0.28	0.28	14.4	313	248	60
Gusev Plains Basalts[c]																
A034	2.41	10.83	10.87	45.7	0.52	1.23	0.20	0.07	7.75	0.48	0.61	0.41	18.8	165	81	14
A060	2.54	10.41	10.68	45.9	0.56	1.28	0.26	0.10	7.84	0.55	0.60	0.41	18.8	164	112	52
A086	2.78	9.72	10.70	45.8	0.65	1.48	0.23	0.16	8.02	0.59	0.54	0.42	18.9	132	75	161
Gusev Clovis Class Rocks																
A195	3.41	8.54	9.68	44.8	0.96	7.33	1.08	0.40	5.62	0.89	0.24	0.20	16.7	516	193	185
A197	3.33	10.92	12.60	46.8	1.24	2.87	0.78	0.07	3.64	0.94	0.27	0.10	16.3	607	89	318
A199	2.92	11.62	10.34	46.4	1.20	2.41	1.03	0.04	3.44	0.91	0.18	0.13	19.2	553	54	493
A214	3.46	8.80	9.66	44.9	1.02	7.77	1.23	0.42	6.15	0.85	0.19	0.27	15.0	562	175	908
A216	3.55	10.79	9.34	43.4	1.13	7.98	1.88	0.35	5.86	0.75	0.18	0.27	14.3	538	107	901
A218	3.64	11.52	8.95	42.2	1.05	7.53	1.63	0.35	6.04	0.84	0.17	0.30	15.6	735	118	239
A225	3.02	11.46	8.85	42.6	0.81	9.29	1.74	0.45	5.39	0.84	0.18	0.23	14.9	670	99	993
A228	2.87	11.16	10.71	47.4	0.94	4.67	1.33	0.36	4.24	0.79	0.14	0.21	15.1	453	146	193
A229	3.20	10.89	10.40	46.8	1.00	5.18	1.32	0.35	4.31	0.78	0.17	0.17	15.3	478	92	267
A231	2.59	13.57	9.93	47.5	0.97	3.81	1.54	0.32	3.63	0.76	0.16	0.15	15.0	497	72	293
A232	2.32	14.82	9.28	47.4	0.97	3.20	1.46	0.33	3.44	0.79	0.16	0.16	15.6	523	99	222
A235	3.01	13.49	10.18	45.3	0.94	3.01	1.38	0.30	3.93	0.90	0.18	0.18	17.1	731	56	352
A266	3.27	9.06	9.47	45.3	0.98	7.37	1.33	0.41	5.75	0.85	0.19	0.35	15.4	568	175	1543
A274	3.31	9.49	10.10	46.4	0.91	6.52	1.42	0.43	5.18	0.86	0.20	0.28	14.7	558	204	694
A284	3.21	9.14	9.74	45.1	0.98	7.38	1.32	0.43	5.90	0.86	0.19	0.30	15.2	564	206	735
A287	2.44	14.28	9.52	45.6	0.94	5.26	1.85	0.35	4.48	0.80	0.15	0.25	13.9	593	118	674
A291	2.82	12.14	9.96	45.4	1.04	5.92	2.62	0.40	4.39	0.80	0.16	0.23	13.9	547	158	903
A300	2.56	14.34	10.29	46.0	0.95	3.44	2.02	0.29	4.59	0.80	0.16	0.17	14.2	629	103	581
A304	2.45	15.12	10.17	45.5	1.04	3.05	2.47	0.24	4.62	0.78	0.16	0.18	14.1	605	112	339
Gusev Wishstone and Watchtower Class Rocks																
A334	5.12	4.94	15.64	46.3	2.63	3.47	0.59	0.54	6.86	2.16	0.01	0.22	11.5	99	96	14
A335	4.98	4.50	15.03	43.8	5.19	2.20	0.35	0.57	8.89	2.59	0.00	0.22	11.6	67	64	22
A349	4.48	5.64	14.68	47.0	1.74	4.10	0.71	0.56	6.62	1.86	0.03	0.25	12.2	57	122	58
A353	4.20	6.15	13.48	46.4	1.79	4.40	0.72	0.53	6.67	1.97	0.04	0.25	13.3	86	105	54
A355	5.30	4.56	15.75	45.8	2.64	2.50	0.62	0.51	6.59	2.84	0.00	0.22	12.6	41	71	38
A356	5.04	3.94	14.86	43.4	5.07	1.94	0.60	0.53	8.78	2.99	0.00	0.24	12.5	24	81	72
A357	5.02	3.98	14.83	43.5	5.05	1.96	0.60	0.53	8.75	2.96	0.00	0.25	12.5	45	58	68
A416	2.78	10.10	12.22	44.1	2.72	4.70	1.14	0.76	6.06	1.89	0.00	0.22	13.3	58	132	262
A417	2.67	10.00	12.33	42.4	4.50	3.43	0.80	0.74	7.44	2.21	0.00	0.22	13.2	67	140	251
A469	3.32	8.38	12.44	47.0	1.23	4.95	0.92	0.51	5.75	2.21	0.11	0.31	12.8	155	117	232
A470	3.44	8.48	13.61	46.9	2.41	4.15	1.23	0.56	6.36	1.96	0.05	0.27	10.5	92	81	204
A475	3.32	8.30	12.49	44.6	3.17	4.73	1.36	0.45	7.40	1.90	0.05	0.21	12.0	147	100	460
A481	3.48	8.16	12.52	46.3	2.62	4.92	1.06	0.40	7.02	1.52	0.13	0.24	11.5	184	97	208
A484	3.60	8.64	12.07	45.2	2.51	6.43	1.28	0.37	6.71	1.94	0.04	0.22	10.9	83	89	302
A491	3.42	7.91	13.73	46.8	2.31	4.97	1.05	0.37	6.45	1.37	0.02	0.17	11.4	74	76	151
A495	3.42	7.82	13.37	46.4	2.68	4.33	0.96	0.39	7.15	1.99	0.06	0.19	11.1	114	88	243

Table 1a. (continued)

Sample	Na_2O	MgO	Al_2O_3	SiO_2	P_2O_5	SO_3	Cl	K_2O	CaO	TiO_2	Cr_2O_3	MnO	FeO	Ni	Zn	Br
A496	3.48	8.42	13.10	46.0	2.83	4.29	0.98	0.38	7.13	1.92	0.05	0.20	11.1	94	80	250
A499	3.45	7.98	12.62	45.8	2.56	4.81	1.02	0.43	7.03	1.83	0.08	0.21	12.1	137	96	197
A630	4.00	7.90	13.37	46.8	2.35	4.55	1.17	0.54	5.93	1.91	0.02	0.21	11.2	51	121	262
A633	4.06	6.98	13.69	46.5	2.79	4.22	1.18	0.52	6.19	2.24	0.01	0.19	11.4	53	113	342
							Gusev Mafic/Ultramafic Rock Sequence									
A630	4.00	7.90	13.37	46.8	2.35	4.55	1.17	0.54	5.93	1.91	0.02	0.21	11.2	51	121	262
A633	4.06	6.98	13.69	46.5	2.79	4.22	1.18	0.52	6.19	2.24	0.01	0.19	11.4	53	113	342
A646	3.41	8.58	9.35	44.0	2.24	7.81	2.08	0.41	6.17	2.12	0.08	0.29	13.4	220	270	235
A660	2.78	11.18	8.49	39.7	2.89	4.80	0.93	0.54	6.40	1.19	0.19	0.37	20.5	229	196	64
A672	2.78	13.80	7.05	43.0	0.90	4.59	1.45	0.94	4.00	0.65	0.42	0.36	20.0	538	235	171
A675	2.98	12.38	7.72	44.1	0.91	4.65	1.24	0.66	4.66	0.61	0.39	0.36	19.3	545	204	126
A687	2.49	13.57	7.29	42.6	0.78	5.62	0.79	0.26	4.12	0.53	0.73	0.39	20.7	858	169	69
A688	1.59	22.30	4.00	40.6	0.63	4.32	0.87	0.12	2.61	0.35	0.87	0.38	21.2	891	131	72
A699	2.43	14.22	6.98	41.9	0.73	5.14	0.70	0.24	4.02	0.51	0.66	0.44	21.9	867	166	153
A700	1.12	24.75	2.93	41.3	0.45	2.69	0.61	0.04	1.93	0.25	0.71	0.43	22.6	1000	132	156
							Meridiani Basaltic Soils[d]									
B011	1.83	7.58	9.26	46.3	0.83	4.99	0.63	0.47	7.31	1.04	0.45	0.37	18.8	423	241	32
B025	2.03	7.49	9.21	45.9	0.80	6.96	0.70	0.49	6.69	1.13	0.40	0.35	17.7	634	428	159
B026	1.92	7.42	9.05	45.3	0.75	5.69	0.59	0.45	6.72	1.24	0.46	0.36	19.9	631	348	130
B060	2.24	7.63	9.22	45.3	0.94	7.34	0.79	0.48	6.59	1.02	0.33	0.34	17.6	470	404	26
B081	2.34	7.59	9.88	47.1	0.74	4.57	0.49	0.41	6.73	1.23	0.48	0.36	17.9	592	256	40
B090	2.35	7.78	9.25	45.6	0.86	5.81	0.60	0.44	6.70	1.09	0.46	0.38	18.5	456	320	232
B123	2.38	7.61	9.21	45.3	0.87	7.12	0.84	0.51	6.73	0.97	0.36	0.37	17.6	503	376	35
B166	2.40	7.14	10.04	47.7	0.81	5.19	0.64	0.55	7.32	0.85	0.34	0.39	16.6	339	226	25
B237	2.39	6.90	10.41	48.8	0.84	4.56	0.58	0.59	7.38	0.85	0.28	0.35	15.9	323	178	21
B249	2.39	7.65	9.59	46.7	0.85	4.62	0.59	0.48	7.30	0.91	0.45	0.40	18.0	344	184	24
B499	2.32	7.05	8.74	44.8	0.91	6.59	0.72	0.47	7.06	1.02	0.41	0.39	19.4	445	298	130
B507	2.13	7.02	8.70	44.1	0.94	7.36	0.76	0.50	6.75	1.05	0.35	0.37	19.8	463	452	121
							Meridiani Hematitic Soils									
B023	2.12	7.50	8.59	42.7	0.81	4.77	0.68	0.43	6.13	0.78	0.30	0.31	24.8	633	312	37
B046	2.29	6.82	8.02	39.5	0.76	5.60	0.72	0.38	5.24	0.70	0.27	0.27	29.3	801	331	41
B080	2.21	6.81	7.66	38.6	0.77	4.90	0.68	0.37	5.10	0.68	0.30	0.27	31.5	882	304	35
B091	2.34	7.27	7.67	38.8	0.82	4.83	0.70	0.34	4.93	0.70	0.28	0.28	30.9	1089	361	53
B100	2.44	6.89	7.82	39.2	0.82	5.95	0.77	0.38	5.14	0.72	0.25	0.28	29.2	773	331	46
B369	2.13	6.39	7.36	37.4	0.87	4.64	0.71	0.33	4.88	0.67	0.27	0.29	33.8	1292	357	101
B370	2.17	6.61	7.83	39.8	0.82	5.05	0.68	0.40	5.67	0.78	0.32	0.29	29.4	750	300	47
B416	2.21	6.75	8.19	41.5	0.86	5.21	0.67	0.42	6.17	0.85	0.33	0.33	26.3	608	282	39
B420A	2.11	6.67	7.72	39.5	0.88	5.90	0.72	0.39	5.30	0.80	0.28	0.29	29.3	850	371	73
B420B	2.19	6.61	7.76	39.0	0.84	5.15	0.70	0.36	5.27	0.78	0.27	0.29	30.6	965	348	96
B443	2.01	6.43	7.78	40.0	0.83	5.54	0.72	0.43	5.69	0.79	0.32	0.32	29.0	729	354	48
B505	2.15	6.54	7.80	39.3	0.82	5.24	0.65	0.39	5.39	0.75	0.32	0.28	30.2	743	331	48
B509	2.18	6.37	7.94	39.9	0.80	5.07	0.66	0.42	5.54	0.73	0.29	0.26	29.7	865	328	45
							Meridiani outcrop: RATted Interior Measurements[e]									
B031	1.67	8.00	6.20	38.3	0.99	21.31	0.60	0.56	4.42	0.81	0.19	0.30	16.5	735	279	342
B036	1.66	8.45	5.85	36.2	0.97	24.91	0.50	0.53	4.91	0.65	0.17	0.30	14.8	589	324	30
B045	1.64	8.38	6.18	36.3	1.01	23.61	0.54	0.59	5.19	0.74	0.20	0.26	15.3	656	427	105
B087	1.50	8.63	5.82	34.7	0.97	25.21	0.66	0.50	4.82	0.76	0.19	0.36	15.7	634	526	33
B108	1.72	8.80	6.22	37.2	1.01	22.84	0.91	0.58	5.03	0.77	0.18	0.29	14.3	572	415	268
B139	1.36	8.38	5.87	35.0	1.03	24.94	0.65	0.58	5.03	0.79	0.20	0.32	15.7	679	533	35
B145	1.54	9.20	5.90	35.9	1.05	24.38	0.65	0.57	4.72	0.71	0.18	0.33	14.7	618	371	54
B147	1.83	9.00	6.32	36.9	1.07	22.09	0.60	0.60	4.43	0.84	0.21	0.39	15.5	664	381	74
B149	1.64	9.14	5.99	36.4	1.11	23.71	0.72	0.57	4.85	0.74	0.20	0.31	14.5	638	357	27
B153	1.70	8.38	6.36	38.0	1.07	21.50	1.45	0.58	4.64	0.83	0.19	0.33	14.8	604	319	39
B155	1.45	8.63	5.85	36.2	1.03	23.03	1.75	0.55	4.85	0.80	0.20	0.33	15.2	644	346	19
B162	1.58	7.41	6.20	37.6	1.17	21.11	1.98	0.59	5.11	0.75	0.21	0.31	15.8	616	437	11
B178	1.72	6.47	6.71	40.6	1.05	19.62	1.37	0.63	5.09	0.79	0.17	0.33	15.4	531	444	23
B180	1.71	6.49	6.70	40.1	1.06	19.64	1.64	0.63	5.03	0.81	0.22	0.31	15.5	611	486	14
B184	1.93	5.43	7.27	43.0	1.15	17.01	1.90	0.69	4.60	0.86	0.20	0.32	15.6	546	447	9
B187	1.79	5.45	7.17	39.9	1.11	18.17	1.67	0.67	5.48	0.86	0.22	0.36	17.1	606	489	13
B195	1.86	6.81	6.52	37.9	1.01	19.33	1.69	0.60	5.01	0.77	0.23	0.37	17.7	933	499	10
B220	1.63	8.37	6.06	36.5	1.01	23.03	0.78	0.57	5.00	0.75	0.18	0.24	15.7	564	314	425
B307	1.84	7.86	6.36	37.7	1.13	21.35	1.42	0.57	4.59	0.77	0.16	0.33	15.7	571	628	10
B312	1.83	9.11	6.43	37.5	1.08	21.33	1.49	0.56	4.10	0.81	0.20	0.32	15.1	605	259	38
B403	1.35	7.33	4.90	32.6	1.07	28.62	0.61	0.51	5.78	0.68	0.17	0.35	15.9	585	436	54
B548	1.74	7.31	5.91	36.2	1.04	23.81	0.64	0.58	5.49	0.78	0.21	0.31	15.8	449	480	109
B558	1.57	8.09	5.72	32.8	0.99	27.39	0.57	0.50	5.13	0.72	0.19	0.39	15.8	504	563	84
B560	2.02	7.83	6.17	35.1	1.05	23.12	1.54	0.54	5.20	0.75	0.19	0.38	16.0	508	457	67

Table 1a. (continued)

Sample	Na_2O	MgO	Al_2O_3	SiO_2	P_2O_5	SO_3	Cl	K_2O	CaO	TiO_2	Cr_2O_3	MnO	FeO	Ni	Zn	Br
B634	1.78	7.39	6.52	37.5	0.98	20.72	0.56	0.55	5.84	0.79	0.25	0.33	16.6	496	394	67
B696	1.51	7.08	5.40	34.6	1.01	26.52	0.46	0.55	5.74	0.71	0.18	0.32	15.8	537	554	182
Meridiani Outcrop: Brushed and Undisturbed Surfaces[f]																
B015	1.56	8.29	7.46	39.6	0.97	19.42	0.81	0.57	5.03	0.74	0.19	0.28	15.0	597	569	7
B029	2.28	8.14	8.39	43.1	0.97	12.73	0.87	0.53	5.72	0.87	0.26	0.30	15.7	588	295	211
B030	1.88	7.95	7.26	40.3	1.01	18.75	0.87	0.58	4.92	0.84	0.17	0.30	15.1	657	373	43
B040	2.09	7.65	7.06	38.4	1.00	18.91	0.90	0.56	4.84	0.70	0.16	0.30	17.4	686	397	32
B041	2.40	8.10	8.75	43.9	0.97	11.42	0.84	0.55	5.70	0.94	0.29	0.33	15.6	625	292	346
B043	2.26	7.82	8.39	43.0	0.98	12.97	0.86	0.56	5.98	0.88	0.23	0.29	15.6	633	414	90
B048	2.11	7.86	8.12	42.7	0.97	14.08	0.99	0.56	5.51	0.84	0.20	0.34	15.6	607	426	103
B049	2.29	8.41	8.34	41.4	1.01	15.19	0.93	0.61	5.29	0.84	0.16	0.27	15.1	553	460	177
B051	2.16	8.16	6.99	38.3	0.99	18.70	0.85	0.52	4.37	0.67	0.17	0.24	17.7	653	388	100
B106	1.98	8.03	7.21	39.7	0.98	18.80	1.00	0.57	5.11	0.78	0.19	0.29	15.3	573	389	76
B142	0.88	8.04	7.89	43.2	0.80	13.41	0.83	0.53	6.34	0.92	0.24	0.24	16.5	652	439	139
B283	1.95	7.43	8.47	43.5	0.95	11.93	0.96	0.59	6.79	0.89	0.29	0.33	15.8	417	391	18
B306	1.74	8.08	6.45	38.7	1.09	21.47	1.10	0.54	4.49	0.76	0.18	0.27	14.9	564	624	147
B308	1.68	9.38	6.28	37.0	1.02	21.55	1.07	0.54	4.27	0.76	0.21	0.29	15.8	804	301	103
B311	2.55	7.86	8.63	42.6	0.91	11.14	0.84	0.50	6.33	0.77	0.24	0.28	17.3	466	273	44
B381	1.84	7.15	6.81	38.5	1.05	20.82	0.94	0.57	5.47	0.80	0.20	0.30	15.4	628	585	60
B393	2.00	7.39	7.10	39.4	1.01	19.81	0.89	0.56	5.16	0.83	0.20	0.30	15.3	634	441	53
B400	2.00	7.19	7.54	41.0	1.04	16.51	0.98	0.56	5.46	0.89	0.20	0.34	16.2	543	450	73
B401	1.79	7.25	6.71	38.3	1.03	21.46	0.92	0.57	5.36	0.78	0.17	0.31	15.2	574	405	67
B556	2.22	7.07	7.49	40.2	1.07	15.30	1.49	0.55	6.07	0.89	0.24	0.37	17.0	525	474	67
B593	1.84	7.37	6.84	38.8	1.08	19.53	0.90	0.61	5.49	0.79	0.22	0.28	16.1	576	450	294
B594	1.79	7.45	6.63	38.5	1.05	19.83	0.74	0.58	5.06	0.80	0.19	0.23	17.0	515	423	103
B638	1.73	7.36	6.26	36.9	1.02	23.00	0.84	0.55	5.12	0.76	0.18	0.31	15.8	544	559	74
B675	1.88	7.50	6.93	39.1	1.01	19.62	0.75	0.57	5.45	0.83	0.19	0.25	15.8	549	470	65
B679	2.04	7.27	7.29	40.1	1.03	17.51	0.90	0.57	5.61	0.85	0.21	0.32	16.2	571	541	161
B680	1.93	7.23	6.69	38.2	1.03	20.62	0.80	0.58	5.45	0.78	0.19	0.31	16.0	548	536	177
B686	2.00	7.48	7.00	39.2	1.01	19.06	0.76	0.55	5.23	0.80	0.20	0.29	16.3	561	634	157
Meridiani "Bounce" Rock[g]																
B068	1.66	6.84	10.48	51.6	0.92	0.56	0.10	0.11	12.09	0.74	0.11	0.40	14.4	81	38	39

[a]Data reduction follows techniques described by *Gellert et al.* [2006]. Concentrations are normalized to 100% with all iron as FeO. Accuracies of elemental concentrations are tabulated by *Gellert et al.* [2004]; precisions are listed in Table 1b. Ni, Zn, and Br values are presented in μg/g; all other values are weight percentages.
[b]Not including ferric sulfates, altered trench deposits, short integrations with poor statistics, or samples with significant rock fragments.
[c]Adirondack class rocks, RATted interior measurements only.
[d]Not including short integrations with poor statistics or subsurface deposits with evidence of chemical mobility.
[e]Includes samples with embedded high-Ni spherules.
[f]Not including samples with known rinds/coatings or obvious soil mantle.
[g]RATted data only.

therefore not useful in providing constraints on the extent of meteoritic material at the Martian surface. In addition, Martian meteorites typically contain between 30–70 μg/g Co. CI chondrites thus contain only 7 to 17 times more Co than Martian meteorites. As a result, cobalt is a much less sensitive indicator of meteoritic contamination than nickel.

[17] Attempts to use other elements to help determine the magnitude of meteoritic contributions to the Martian surface were unsuccessful because of either inadequate detection limits or lack of sensitivity to mixtures with small quantities of meteoritic material. The concentrations of iridium, gold, and germanium, which can be diagnostic of a meteoritic input, are far below detection limits. The most useful element for establishing the potential level of exogenic flux is clearly nickel.

3.3. Nickel in the Rock Abrasion Tool (RAT)

[18] The viability of using nickel as a meteoritic tracer is dependent upon the absence of analysis artifacts. The abrasive pads on the MER RAT utilize 120 mesh synthetic diamonds impregnated in a phenolic resin with silicon carbide and cryolite (Na_3AlF_6) fibers [*Myrick et al.*, 2004]. To increase the adhesion characteristics with the resin, the diamond grit is coated with nickel [*Myrick et al.*, 2004]. The abrading capability of the RAT is maintained by exposing fresh diamond as the worn grains fall out. Thus there is a possibility of Ni contamination in APXS measurements of abraded surfaces. However, the decrease in Ni levels from brushed to abraded analyses for the Ni-poor, Wishstone rock sample [*Gellert et al.*, 2006] is an indication that Ni contamination in abraded surfaces is generally negligible. On the basis of specific grind energies calculated from the RAT telemetry [*Bartlett et al.*, 2005], Wishstone is among the harder rocks abraded by the rovers. Even in the hardest rocks encountered by the rovers (Gusev plains basalts, "Adirondack" Class), the differences between the determined Ni concentrations before and after abrading are within the precision of the measurements. Thus, given that brushing operations do not deposit nickel-coated diamonds, and that subsequent abrading of the target, even in the hardest

Table 1b. Two Sigma Statistical Uncertainties Associated With the APXS Data Listed in Table 1a[a]

Sample	Na_2O	MgO	Al_2O_3	SiO_2	P_2O_5	SO_3	Cl	K_2O	CaO	TiO_2	Cr_2O_3	MnO	FeO	Ni	Zn	Br
Gusev Basaltic Soils																
A014	0.23	0.12	0.14	0.44	0.08	0.08	0.02	0.06	0.05	0.07	0.03	0.01	0.11	51	18	17
A041	0.93	0.27	0.29	0.71	0.26	0.17	0.04	0.15	0.12	0.20	0.06	0.06	0.21	100	51	30
A043	0.27	0.15	0.17	0.53	0.09	0.10	0.02	0.06	0.07	0.08	0.04	0.02	0.15	65	27	21
A044	1.25	0.37	0.38	0.92	0.32	0.26	0.06	0.17	0.16	0.23	0.07	0.09	0.29	138	74	39
A045	1.79	0.47	0.36	0.64	0.28	0.21	0.05	0.16	0.14	0.15	0.07	0.07	0.18	135	63	37
A047	0.21	0.11	0.11	0.33	0.08	0.09	0.02	0.06	0.05	0.07	0.03	0.01	0.08	51	20	17
A049	0.25	0.13	0.14	0.47	0.08	0.09	0.02	0.06	0.06	0.08	0.04	0.01	0.12	61	26	21
A050	0.24	0.13	0.16	0.47	0.08	0.08	0.02	0.06	0.05	0.07	0.04	0.01	0.12	56	20	18
A052	0.96	0.28	0.29	0.77	0.26	0.21	0.05	0.15	0.13	0.18	0.06	0.07	0.24	112	53	34
A065	1.03	0.30	0.28	0.75	0.26	0.23	0.05	0.16	0.13	0.16	0.06	0.07	0.24	131	67	10
A071	0.29	0.15	0.16	0.52	0.09	0.13	0.03	0.07	0.07	0.08	0.04	0.02	0.15	73	32	22
A074A	0.25	0.14	0.15	0.48	0.08	0.08	0.02	0.06	0.06	0.07	0.04	0.01	0.13	60	22	19
A074B	1.07	0.24	0.31	0.47	0.34	0.17	0.05	0.15	0.11	0.14	0.06	0.07	0.15	113	53	30
A105	1.19	0.34	0.31	0.82	0.29	0.25	0.05	0.17	0.15	0.18	0.07	0.08	0.25	129	74	35
A113	1.23	0.33	0.26	0.64	0.24	0.18	0.04	0.15	0.11	0.16	0.06	0.06	0.19	108	50	31
A122	1.00	0.29	0.27	0.71	0.26	0.19	0.04	0.15	0.12	0.16	0.06	0.07	0.21	100	48	31
A126	1.65	0.46	0.40	0.83	0.30	0.24	0.05	0.17	0.14	0.19	0.07	0.08	0.25	141	73	10
A135	1.67	0.46	0.37	0.69	0.27	0.16	0.03	0.15	0.11	0.20	0.06	0.06	0.20	95	45	26
A158	0.85	0.26	0.26	0.70	0.23	0.15	0.03	0.15	0.12	0.16	0.06	0.06	0.21	102	45	29
A227	0.90	0.26	0.26	0.68	0.25	0.20	0.04	0.15	0.10	0.14	0.05	0.06	0.20	100	44	37
A259	0.23	0.12	0.14	0.45	0.08	0.09	0.02	0.06	0.05	0.07	0.03	0.01	0.11	48	17	16
A280	0.21	0.12	0.12	0.43	0.08	0.08	0.02	0.06	0.05	0.07	0.03	0.01	0.11	47	15	17
A315	0.31	0.16	0.16	0.50	0.08	0.09	0.02	0.06	0.06	0.07	0.04	0.01	0.12	51	18	17
A342	0.23	0.13	0.14	0.46	0.08	0.08	0.01	0.06	0.06	0.07	0.03	0.01	0.12	52	15	17
A477	0.31	0.15	0.15	0.49	0.08	0.08	0.01	0.06	0.06	0.07	0.03	0.01	0.11	47	16	16
A587	0.28	0.13	0.12	0.42	0.07	0.08	0.01	0.06	0.04	0.06	0.03	0.01	0.10	40	14	15
A588	0.20	0.10	0.11	0.40	0.07	0.08	0.01	0.06	0.04	0.06	0.03	0.01	0.10	39	12	15
A607	0.20	0.10	0.12	0.40	0.07	0.06	0.01	0.06	0.04	0.07	0.03	0.01	0.09	36	10	14
Gusev Plains Basalts																
A034	0.20	0.12	0.12	0.41	0.07	0.03	0.01	0.05	0.05	0.06	0.03	0.01	0.12	39	11	15
A060	0.28	0.14	0.13	0.43	0.07	0.03	0.01	0.05	0.05	0.06	0.03	0.01	0.12	39	11	16
A086	0.20	0.11	0.12	0.41	0.07	0.03	0.01	0.05	0.06	0.06	0.03	0.01	0.12	39	11	17
Gusev Clovis Class Rocks																
A195	0.20	0.11	0.12	0.41	0.07	0.09	0.02	0.06	0.04	0.07	0.03	0.01	0.11	44	13	17
A197	0.22	0.14	0.17	0.44	0.08	0.05	0.02	0.05	0.04	0.07	0.03	0.01	0.11	47	12	20
A199	0.20	0.13	0.12	0.43	0.08	0.04	0.02	0.05	0.03	0.07	0.03	0.01	0.12	46	11	21
A214	0.21	0.11	0.12	0.42	0.08	0.09	0.02	0.06	0.05	0.07	0.03	0.01	0.10	44	12	24
A216	0.23	0.14	0.13	0.42	0.08	0.10	0.03	0.06	0.05	0.07	0.03	0.01	0.10	47	13	26
A218	0.23	0.13	0.10	0.38	0.08	0.10	0.03	0.06	0.05	0.07	0.03	0.01	0.08	55	16	20
A225	1.11	0.30	0.27	0.52	0.36	0.25	0.06	0.15	0.09	0.14	0.05	0.06	0.15	94	33	45
A228	0.75	0.25	0.24	0.67	0.21	0.14	0.05	0.14	0.08	0.13	0.04	0.04	0.18	80	32	29
A229	0.20	0.13	0.12	0.42	0.07	0.07	0.02	0.06	0.04	0.06	0.03	0.01	0.10	41	9	17
A231	0.21	0.15	0.12	0.43	0.07	0.06	0.02	0.06	0.03	0.06	0.03	0.01	0.10	43	10	18
A232	0.22	0.17	0.13	0.45	0.08	0.06	0.02	0.06	0.04	0.07	0.03	0.01	0.11	47	13	19
A235	0.81	0.28	0.24	0.64	0.22	0.12	0.05	0.13	0.08	0.14	0.05	0.04	0.20	93	29	36
A266	0.20	0.11	0.11	0.40	0.07	0.08	0.02	0.06	0.04	0.06	0.03	0.01	0.10	42	11	28
A274	0.22	0.11	0.11	0.40	0.08	0.08	0.02	0.06	0.04	0.07	0.03	0.01	0.08	48	15	23
A284	0.22	0.12	0.12	0.43	0.08	0.09	0.02	0.06	0.05	0.07	0.03	0.01	0.11	47	14	24
A287	0.20	0.13	0.10	0.35	0.07	0.06	0.02	0.06	0.03	0.06	0.03	0.01	0.06	41	9	20
A291	0.22	0.14	0.12	0.42	0.08	0.08	0.03	0.06	0.04	0.07	0.03	0.01	0.10	44	12	24
A300	0.20	0.15	0.12	0.41	0.07	0.05	0.02	0.06	0.04	0.06	0.03	0.01	0.09	42	10	20
A304	0.22	0.17	0.13	0.43	0.08	0.05	0.03	0.06	0.04	0.07	0.03	0.01	0.10	46	12	19
Gusev Wishstone and Watchtower Class Rocks																
A334	0.28	0.14	0.24	0.49	0.11	0.07	0.02	0.06	0.07	0.09	0.03	0.01	0.10	41	14	17
A335	0.25	0.10	0.17	0.44	0.13	0.05	0.01	0.06	0.07	0.10	0.02	0.01	0.10	40	13	16
A349	0.29	0.13	0.21	0.52	0.10	0.09	0.02	0.06	0.07	0.10	0.03	0.01	0.11	48	19	19
A353	0.23	0.10	0.15	0.36	0.09	0.08	0.02	0.06	0.06	0.09	0.03	0.01	0.08	44	15	18
A355	0.21	0.07	0.15	0.38	0.08	0.04	0.01	0.06	0.04	0.08	0.02	0.01	0.08	30	7	13
A356	0.25	0.09	0.17	0.42	0.12	0.04	0.01	0.06	0.07	0.10	0.02	0.01	0.09	40	13	18
A357	0.23	0.08	0.14	0.32	0.11	0.04	0.01	0.06	0.06	0.09	0.02	0.01	0.08	41	13	16
A416	0.27	0.16	0.19	0.48	0.11	0.08	0.03	0.07	0.06	0.09	0.03	0.01	0.11	45	17	21
A417	0.23	0.13	0.15	0.41	0.11	0.06	0.02	0.06	0.06	0.08	0.02	0.01	0.10	37	12	19
A469	0.23	0.11	0.13	0.37	0.08	0.07	0.02	0.06	0.05	0.08	0.03	0.01	0.07	40	13	18
A470	0.21	0.09	0.12	0.34	0.09	0.05	0.02	0.06	0.04	0.07	0.03	0.01	0.05	34	9	16
A475	0.28	0.13	0.15	0.38	0.11	0.09	0.03	0.06	0.07	0.09	0.03	0.01	0.08	47	17	24
A481	0.23	0.11	0.14	0.42	0.09	0.07	0.02	0.06	0.05	0.08	0.03	0.01	0.08	37	10	17
A484	0.22	0.11	0.13	0.40	0.09	0.07	0.02	0.06	0.05	0.08	0.03	0.01	0.07	32	8	17
A491	0.23	0.11	0.15	0.43	0.09	0.07	0.02	0.06	0.05	0.07	0.03	0.01	0.08	35	9	17
A495	0.22	0.11	0.15	0.41	0.09	0.06	0.02	0.06	0.05	0.08	0.03	0.01	0.08	34	9	17

Table 1b. (continued)

Sample	Na_2O	MgO	Al_2O_3	SiO_2	P_2O_5	SO_3	Cl	K_2O	CaO	TiO_2	Cr_2O_3	MnO	FeO	Ni	Zn	Br
A496	0.22	0.11	0.14	0.41	0.09	0.06	0.02	0.06	0.05	0.07	0.03	0.01	0.08	34	9	17
A499	0.22	0.11	0.14	0.41	0.09	0.06	0.02	0.06	0.05	0.08	0.03	0.01	0.08	35	9	17
A630	0.25	0.11	0.15	0.44	0.09	0.07	0.02	0.06	0.05	0.08	0.03	0.01	0.08	37	12	18
A633	0.20	0.08	0.12	0.30	0.09	0.05	0.02	0.06	0.04	0.08	0.03	0.01	0.05	33	9	17
							Gusev Mafic/Ultramafic Rock Sequence									
A630	0.25	0.11	0.15	0.44	0.09	0.07	0.02	0.06	0.05	0.08	0.03	0.01	0.08	37	12	18
A633	0.20	0.08	0.12	0.30	0.09	0.05	0.02	0.06	0.04	0.08	0.03	0.01	0.05	33	9	17
A646	0.21	0.10	0.11	0.39	0.09	0.09	0.02	0.06	0.04	0.08	0.03	0.01	0.09	35	11	17
A660	0.29	0.15	0.13	0.39	0.09	0.07	0.02	0.06	0.05	0.07	0.03	0.01	0.13	40	13	16
A672	0.38	0.19	0.11	0.43	0.07	0.06	0.02	0.06	0.03	0.06	0.03	0.01	0.12	43	12	17
A675	0.21	0.12	0.08	0.30	0.07	0.05	0.02	0.06	0.03	0.06	0.03	0.01	0.09	42	11	15
A687	0.19	0.14	0.09	0.37	0.07	0.07	0.01	0.05	0.03	0.06	0.03	0.01	0.12	44	10	15
A688	0.19	0.20	0.06	0.34	0.07	0.05	0.01	0.05	0.02	0.06	0.03	0.01	0.12	43	9	15
A699	0.19	0.13	0.08	0.30	0.07	0.06	0.01	0.05	0.03	0.06	0.03	0.01	0.10	46	11	16
A700	0.25	0.23	0.08	0.36	0.07	0.04	0.01	0.05	0.02	0.06	0.03	0.01	0.13	49	11	17
							Meridiani Basaltic Soils									
B011	0.28	0.12	0.13	0.47	0.08	0.08	0.02	0.06	0.06	0.07	0.04	0.01	0.13	57	20	17
B025	0.24	0.11	0.12	0.38	0.08	0.09	0.02	0.06	0.06	0.08	0.04	0.01	0.11	61	24	21
B026	0.30	0.13	0.14	0.48	0.08	0.09	0.02	0.06	0.06	0.08	0.04	0.02	0.15	69	28	21
B060	0.19	0.08	0.09	0.29	0.07	0.07	0.01	0.06	0.04	0.07	0.03	0.01	0.07	42	14	14
B081	0.29	0.14	0.15	0.50	0.08	0.08	0.02	0.06	0.07	0.08	0.04	0.02	0.14	66	25	21
B090	0.23	0.11	0.14	0.41	0.07	0.07	0.01	0.06	0.05	0.07	0.03	0.01	0.11	43	14	17
B123	0.30	0.15	0.16	0.50	0.09	0.12	0.02	0.06	0.07	0.08	0.04	0.02	0.14	62	26	19
B166	0.28	0.13	0.15	0.49	0.08	0.09	0.02	0.06	0.06	0.08	0.04	0.01	0.13	52	19	17
B237	0.24	0.11	0.13	0.47	0.07	0.07	0.01	0.06	0.06	0.07	0.03	0.01	0.11	46	14	16
B249	0.22	0.10	0.11	0.35	0.08	0.07	0.01	0.06	0.06	0.07	0.04	0.01	0.10	48	15	16
B499	0.28	0.17	0.20	0.60	0.11	0.16	0.03	0.07	0.10	0.09	0.05	0.03	0.21	87	40	27
B507	0.22	0.12	0.17	0.44	0.08	0.11	0.02	0.06	0.06	0.07	0.04	0.01	0.15	55	23	21
							Meridiani Hematitic Soils									
B023	0.26	0.12	0.13	0.45	0.08	0.08	0.02	0.06	0.06	0.07	0.04	0.01	0.17	64	24	19
B046	0.21	0.09	0.12	0.34	0.07	0.06	0.01	0.06	0.04	0.06	0.03	0.01	0.15	45	13	15
B080	0.27	0.13	0.13	0.47	0.08	0.10	0.02	0.06	0.06	0.07	0.04	0.02	0.24	84	31	23
B091	0.23	0.11	0.11	0.39	0.08	0.08	0.02	0.06	0.05	0.07	0.03	0.01	0.20	66	22	19
B100	0.23	0.11	0.11	0.39	0.08	0.08	0.02	0.06	0.05	0.07	0.03	0.01	0.18	60	20	19
B369	0.20	0.10	0.13	0.37	0.08	0.08	0.02	0.06	0.05	0.07	0.04	0.01	0.22	73	23	21
B370	0.22	0.10	0.10	0.40	0.07	0.07	0.01	0.06	0.05	0.07	0.03	0.01	0.18	56	18	17
B416	0.26	0.13	0.13	0.36	0.08	0.08	0.02	0.06	0.06	0.07	0.04	0.01	0.15	63	22	17
B420A	0.30	0.14	0.12	0.41	0.08	0.09	0.02	0.06	0.05	0.07	0.04	0.01	0.19	63	22	19
B420B	0.20	0.10	0.11	0.41	0.08	0.09	0.02	0.06	0.05	0.07	0.04	0.01	0.21	71	25	21
B443	0.20	0.09	0.11	0.42	0.08	0.09	0.02	0.06	0.06	0.07	0.04	0.02	0.20	75	28	20
B505	0.18	0.09	0.10	0.38	0.07	0.07	0.02	0.06	0.05	0.07	0.03	0.01	0.19	61	20	17
B509	0.18	0.08	0.09	0.29	0.07	0.07	0.02	0.06	0.05	0.07	0.03	0.01	0.13	64	21	17
							Meridiani Outcrop: RATted Interior Measurements									
B031	0.27	0.13	0.12	0.40	0.09	0.22	0.02	0.06	0.05	0.08	0.03	0.01	0.12	56	19	21
B036	0.26	0.12	0.10	0.37	0.09	0.25	0.01	0.06	0.05	0.07	0.03	0.01	0.11	50	17	16
B045	0.27	0.13	0.10	0.38	0.09	0.24	0.02	0.06	0.05	0.07	0.03	0.01	0.12	54	21	19
B087	0.22	0.11	0.08	0.33	0.08	0.22	0.01	0.06	0.04	0.06	0.03	0.01	0.10	45	16	15
B108	0.32	0.15	0.11	0.39	0.09	0.24	0.02	0.06	0.05	0.08	0.03	0.01	0.11	52	19	20
B139	0.24	0.11	0.11	0.33	0.08	0.22	0.01	0.06	0.04	0.07	0.03	0.01	0.10	47	17	15
B145	0.39	0.17	0.12	0.39	0.09	0.26	0.02	0.06	0.05	0.07	0.03	0.01	0.12	55	20	17
B147	0.29	0.14	0.11	0.40	0.09	0.24	0.02	0.06	0.05	0.07	0.03	0.01	0.12	58	22	18
B149	0.28	0.15	0.11	0.40	0.09	0.26	0.02	0.06	0.05	0.07	0.03	0.01	0.12	57	21	18
B153	0.28	0.13	0.11	0.39	0.09	0.23	0.03	0.06	0.05	0.07	0.03	0.01	0.11	53	18	17
B155	0.31	0.15	0.11	0.39	0.09	0.26	0.03	0.06	0.05	0.08	0.04	0.01	0.12	59	22	17
B162	0.29	0.13	0.11	0.41	0.09	0.24	0.04	0.06	0.05	0.08	0.04	0.01	0.13	59	24	19
B178	0.23	0.10	0.10	0.34	0.08	0.19	0.03	0.06	0.05	0.07	0.03	0.01	0.09	52	20	16
B180	0.31	0.14	0.13	0.44	0.09	0.23	0.03	0.06	0.06	0.07	0.04	0.01	0.13	61	26	19
B184	0.31	0.13	0.13	0.46	0.09	0.21	0.03	0.06	0.05	0.08	0.04	0.01	0.12	58	24	17
B187	0.25	0.11	0.11	0.37	0.09	0.20	0.03	0.07	0.06	0.08	0.04	0.01	0.12	64	27	18
B195	0.29	0.13	0.12	0.42	0.09	0.23	0.03	0.06	0.05	0.07	0.04	0.02	0.14	67	26	19
B220	0.28	0.13	0.11	0.39	0.09	0.25	0.02	0.06	0.05	0.07	0.03	0.01	0.12	55	19	24
B307	0.31	0.15	0.12	0.44	0.09	0.26	0.03	0.06	0.06	0.07	0.04	0.02	0.14	62	29	17
B312	0.27	0.14	0.11	0.40	0.09	0.23	0.03	0.06	0.05	0.07	0.03	0.01	0.12	55	18	18
B403	0.20	0.10	0.08	0.32	0.09	0.28	0.02	0.06	0.06	0.08	0.03	0.01	0.11	56	22	17
B548	0.18	0.08	0.07	0.25	0.07	0.17	0.01	0.06	0.04	0.06	0.03	0.01	0.07	41	14	15
B558	0.17	0.09	0.07	0.29	0.07	0.22	0.01	0.06	0.04	0.06	0.03	0.01	0.10	39	14	15
B560	0.22	0.10	0.08	0.32	0.08	0.20	0.02	0.06	0.04	0.06	0.03	0.01	0.10	41	14	15

Table 1b. (continued)

Sample	Na_2O	MgO	Al_2O_3	SiO_2	P_2O_5	SO_3	Cl	K_2O	CaO	TiO_2	Cr_2O_3	MnO	FeO	Ni	Zn	Br
B634	0.22	0.10	0.09	0.35	0.08	0.18	0.01	0.06	0.04	0.07	0.03	0.01	0.10	42	14	15
B696	0.22	0.11	0.09	0.36	0.09	0.27	0.02	0.06	0.05	0.07	0.03	0.01	0.12	55	23	20
Meridiani Outcrop: Brushed and Undisturbed Surfaces																
B015	0.88	0.21	0.18	0.49	0.19	0.28	0.03	0.07	0.07	0.12	0.04	0.04	0.14	72	34	21
B029	0.25	0.12	0.12	0.41	0.08	0.14	0.02	0.06	0.05	0.07	0.03	0.01	0.11	49	16	18
B030	0.30	0.14	0.12	0.44	0.09	0.22	0.02	0.06	0.05	0.08	0.04	0.01	0.12	60	23	19
B040	0.23	0.10	0.09	0.36	0.08	0.18	0.02	0.06	0.04	0.06	0.03	0.01	0.11	48	16	15
B041	1.36	0.35	0.35	0.76	0.30	0.31	0.05	0.08	0.11	0.24	0.06	0.08	0.21	109	49	39
B043	0.25	0.12	0.12	0.43	0.08	0.15	0.02	0.06	0.05	0.07	0.03	0.01	0.11	52	19	17
B048	0.27	0.13	0.12	0.44	0.08	0.16	0.02	0.06	0.05	0.07	0.03	0.01	0.12	53	21	19
B049	1.06	0.31	0.27	0.65	0.25	0.37	0.06	0.08	0.12	0.22	0.06	0.07	0.21	119	63	36
B051	0.25	0.13	0.11	0.40	0.08	0.20	0.02	0.06	0.05	0.07	0.03	0.01	0.13	55	21	18
B106	0.25	0.12	0.11	0.39	0.08	0.19	0.02	0.06	0.04	0.07	0.03	0.01	0.11	48	17	16
B142	2.77	0.49	0.48	0.95	0.49	0.36	0.07	0.09	0.14	0.24	0.07	0.11	0.23	127	62	35
B283	0.35	0.17	0.17	0.53	0.10	0.19	0.03	0.07	0.08	0.08	0.04	0.02	0.15	74	33	22
B306	0.27	0.13	0.14	0.41	0.09	0.23	0.02	0.06	0.05	0.08	0.03	0.01	0.11	51	22	18
B308	0.27	0.14	0.11	0.40	0.09	0.24	0.02	0.06	0.05	0.07	0.03	0.01	0.12	58	19	18
B311	0.28	0.14	0.17	0.45	0.09	0.15	0.02	0.06	0.06	0.07	0.03	0.01	0.13	55	20	18
B381	0.20	0.10	0.10	0.36	0.08	0.21	0.02	0.06	0.05	0.07	0.03	0.01	0.11	51	21	16
B393	0.22	0.12	0.14	0.42	0.09	0.23	0.02	0.06	0.06	0.07	0.03	0.01	0.13	58	23	18
B400	0.28	0.13	0.12	0.43	0.09	0.19	0.02	0.06	0.06	0.08	0.03	0.01	0.13	56	23	19
B401	0.28	0.13	0.12	0.40	0.09	0.23	0.02	0.06	0.05	0.07	0.03	0.01	0.12	55	21	18
B556	0.16	0.07	0.07	0.25	0.07	0.12	0.02	0.06	0.04	0.06	0.03	0.01	0.06	41	14	14
B593	0.24	0.13	0.13	0.44	0.10	0.25	0.03	0.07	0.07	0.09	0.04	0.02	0.14	66	29	24
B594	0.17	0.09	0.08	0.30	0.07	0.16	0.01	0.06	0.04	0.07	0.03	0.01	0.09	46	16	16
B638	0.16	0.07	0.06	0.23	0.07	0.16	0.01	0.06	0.03	0.06	0.03	0.01	0.06	39	13	14
B675	0.18	0.09	0.09	0.35	0.08	0.18	0.01	0.06	0.04	0.07	0.03	0.01	0.10	44	15	15
B679	0.31	0.15	0.14	0.44	0.09	0.21	0.02	0.06	0.06	0.07	0.04	0.02	0.14	59	26	21
B680	0.16	0.07	0.07	0.24	0.07	0.15	0.01	0.06	0.04	0.06	0.03	0.01	0.06	40	13	15
B686	0.22	0.10	0.09	0.35	0.07	0.16	0.01	0.06	0.04	0.06	0.03	0.01	0.10	40	15	16
Meridiani "Bounce" Rock																
B068	0.25	0.11	0.14	0.51	0.08	0.03	0.01	0.05	0.09	0.07	0.03	0.01	0.11	42	12	17

[a]These values are representative of the precision of the analyses. Ni, Zn, and Br values are presented in μg/g; all other values are weight percentages.

rocks, did not increase the Ni-concentration relative to the brushed surface, the addition of Ni to the sample by the RAT abrasion must be insignificant.

4. Abundance of Nickel

[19] In constraining the extent of meteoritic contributions to the Martian surface, it is not appropriate to simply assume that materials with low nickel concentrations are indigenous to Mars while higher Ni levels represent exogenic contamination. A number of factors, including the possible presence of high-Ni magmas and redistribution in aqueous solutions affect the observed Ni levels. Table 2 presents an approximate ordering of Ni content of various groupings of Martian rocks and soils.

4.1. Fe-Ni and Stony Meteorites

[20] The upper end of Ni concentrations in Table 2 represents samples that are entirely meteoritic. As discussed above, the Meridiani Planum "Heatshield Rock" is a IAB iron meteorite, and the Barberton pebble is likely a meteorite as well.

4.2. Younger Basalts

[21] Interpretation of the low end of Ni concentrations in Table 2 is also straightforward. These are clearly volcanic rocks, and there is no reason to suspect contamination from meteoritic debris in the measurements. The Adirondack Class rocks are ubiquitous on the Gusev plains and are classified as picritic basalts similar to olivine-phyric shergottites [*McSween et al.*, 2006a]. Backstay (trachybasalt), Irvine (basalt), and Wishstone (trachyte) are relatively unaltered and may have formed during fractional crystallization of Adirondack-class magmas [*McSween et al.*, 2006b]. Bounce rock at Meridiani is a pyroxene-rich volcanic rock similar to basaltic shergottites EETA 79001 lithology B and QUE 94201 [*Zipfel et al.*, 2004]. These rocks all have Ni concentrations less than 300 ppm, which is inadequate to directly account for the Ni levels in the soils and in sedimentary rocks such as the Meridiani outcrop rocks.

[22] These Ni concentrations are consistent with predictions of the bulk composition of the Martian primitive mantle (present mantle plus core), which may differ significantly from that of the Earth [*Halliday et al.*, 2001]. Mars is widely viewed to be an iron- and moderately volatile element-enriched planet. The Martian primitive mantle also may be depleted in S, which was extracted into the early-formed core. This history has led to depletion of the moderately volatile siderophile elements, including nickel and to a lesser degree cobalt. Accordingly, *Wänke* [1991] proposed a primitive mantle Ni content of 400 ppm, about a factor of five less than that of the Earth.

4.3. Ancient Mafic/Ultramafic Sequence

[23] In contrast to the younger basalts, high-Ni magmas are suggested in a series of rock outcrops analyzed by Spirit in the descent from Husband Hill. As introduced in

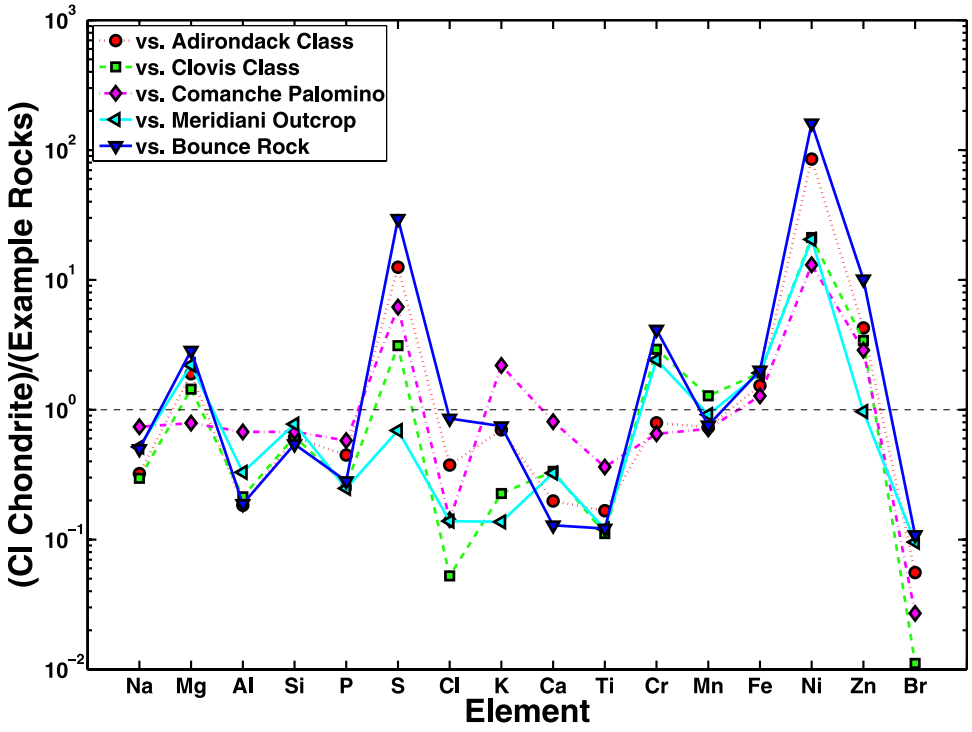

Figure 4. CI chondrite composition normalized to selected Martian rocks. CI chondrites have large excesses in Ni compared to all samples analyzed by the MER rovers. Mg, S, K, Cr, Mn, Fe, and Zn are enriched in CIs compared to certain samples, but the enrichment factor is generally substantially less than that for Ni. CI data [*Lodders*, 2003] are recomputed to an oxide sum of 100% to be consistent with MER APXS data.

Table 2. Samples Grouped by Increasing Nickel Content[a]

Group/Sample	Rover	Approximate Range, ppm	Comments
		Low Ni	
Wishstone Class	A	30–70	Volcanic rocks indigenous to Mars which are unlikely to contain meteoritic material.
Bounce rock	B	80	
Watchtower Class	A	50–150	
Adirondack Class	A	150	
Backstay	A	200	
Kansas/Larry'sBench	A	200	
Irvine	A	290	
Mars meteorites (exc. Chassigny)	-	30–330	
Chassigny (dunite)	-	460	
		Intermediate Ni	
Home Plate	A	300–400	Could contain meteoritic nickel. Elevated Ni concentrations due to formation from a Ni-rich magma and/or enhanced Ni concentrations through aqueous transport are also possible.
Basaltic soils	A/B	300–650	
Seminole	A	550	
Meridiani outcrop	B	500–650	
Clovis Class	A	500–700	
Peace Class	A	600–750	
PasoRobles "class"	A	100–900	
Pot of Gold region	A	700–900	
Algonquin/Comanche	A	850–1000	
Hematite-rich soils	B	600–1300	
Assemblee/Independence	A	450–2100	
		High Ni	
Barberton	B	1700	Meteoritic samples.
CI Chondrites (volatile free)	-	13100	
Heatshield rock	B	70000	

[a]Rovers "A" and "B" represent data from Spirit and Opportunity, respectively. Refer to text and *Squyres et al.* [2006] for descriptions of the sample groups.

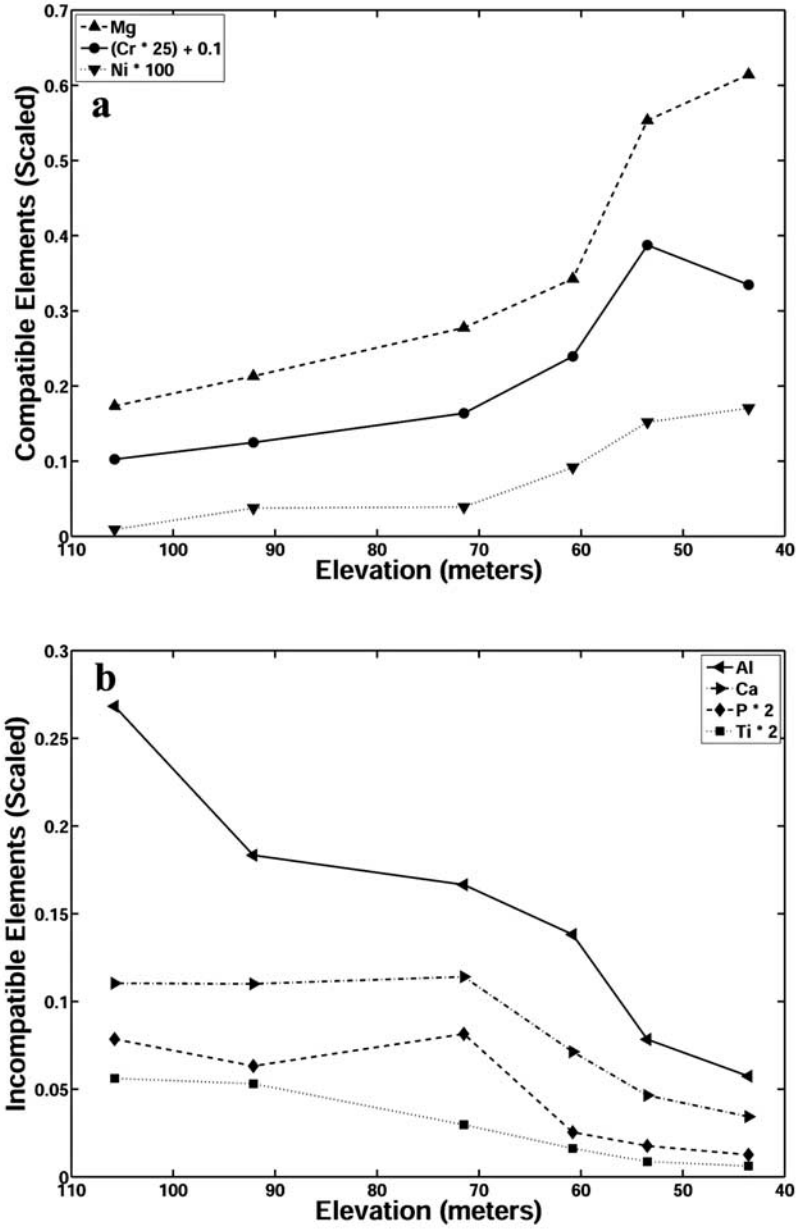

Figure 5. Molar element trends along the downhill traverse from the summit of Husband Hill. The elevation is indicated in meters above the lander. Samples from highest elevation to lowest: Hillary (summit), Kansas, Larry's Bench, Seminole, Algonquin, and Comanche. In cases where multiple analyses of a sample were acquired, the data point with the lower sulfur content (less dust) is plotted here. Elements are scaled as indicated in the legend for clarity. Error bars representing the precision of the APXS analyses are within the marker for each data point. (a) Compatible elements generally increase downhill. (b) Incompatible elements generally decrease downhill.

Mittlefehldt et al. [2006], the set of targets from Larry's Bench, to Seminole, to Algonquin, to Comanche represents a possible mafic-ultramafic magmatic sequence. Analyses from samples progressively further downhill exhibit a systematic increase in compatible elements Mg, Cr, and Ni, while Al, P, Ca, and Ti decrease [*Mittlefehldt et al.*, 2006]. These geochemical trends are unlikely to occur as a product of impact mixing or aqueous weathering. The likelihood that this is an igneous sequence is important in this discussion because the Comanche sample exhibits a relatively high Ni concentration (1000 ppm). That is, if Mars is inherently high in Ni, a meteoritic component might not be necessary to account for the Ni in soils and sedimentary rocks.

[24] To further explore this possibility, the data points considered by *Mittlefehldt et al.* [2006] are extended uphill to include the targets Kansas and the summit of Husband Hill (Hillary). Figure 5 plots the behavior of the compatible and incompatible elements versus vertical elevation. The trends do in fact continue uphill beyond the Larry's Bench target. The leveling off of the P and Ca trend lines for the uphill samples might be a result of the removal of apatite at

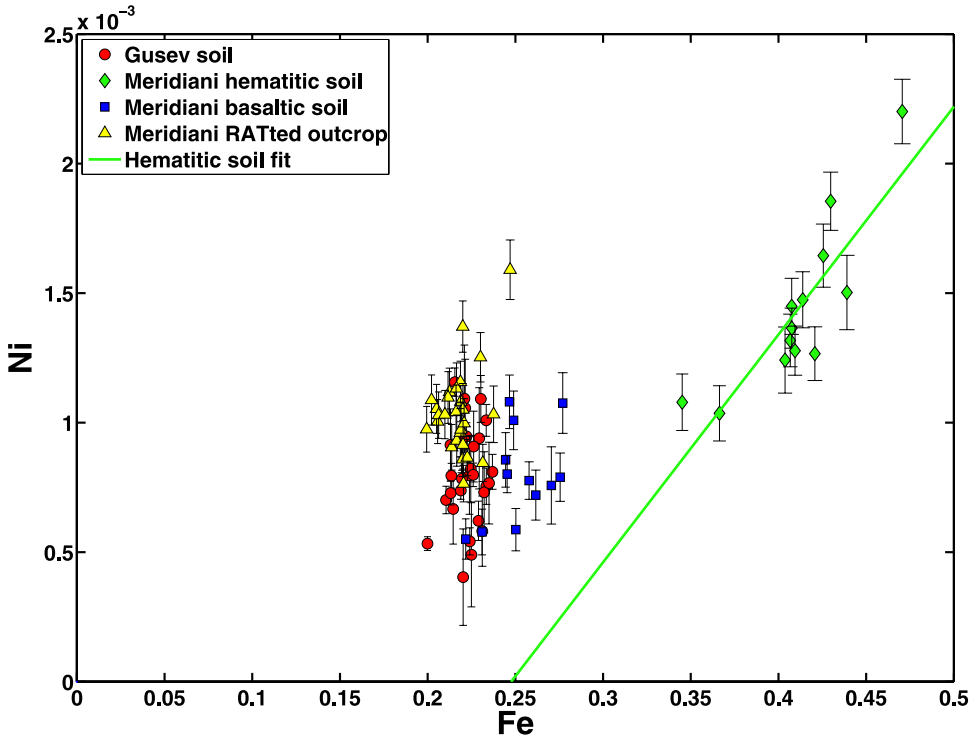

Figure 6. Molar Ni versus Fe showing positive correlation for hematitic spherules at Meridiani. Error bars represent 2-sigma precision of the APXS analyses.

the surfaces of the Hillary and Kansas targets, a weathering process which has been described by *Gellert et al.* [2006] and *Hurowitz et al.* [2006]. Kansas also has a residual of almost 8 wt% SO_3 after brushing by the RAT. This is an indication of surface dust contamination and/or an altered coating, which will also affect the fidelity of the measurements. Nonetheless, a definite trend in compatible and incompatible elements extends across 6 data points covering ~60 meters of vertical relief. Such a pattern should not exist at random and provides strong evidence for a fractional crystallization process. This trend indicates that there may be examples of indigenous Martian rocks that are rich in Ni, making it more difficult to constrain the extent of meteoritic influx based solely on the Ni abundance.

4.4. Mobility in Solution

[25] Further complicating this story is the issue of aqueous weathering. Ni is soluble in chloride brines [*Rose and Bianchimosquera*, 1993] and could therefore be redistributed and concentrated in certain samples. On the other hand, relatively little research has been carried out on the aqueous geochemistry of Ni, especially under conditions relevant to Mars where acid-sulfate weathering may be dominant.

[26] The Independence, Assemblee, and Ben's Clod targets analyzed by Spirit exhibit low Fe, high Al/Si, and highly irregular concentrations of trace elements (including more than 2000 ppm Ni in one measurement). These characteristics are consistent with the initial development of smectite-like clay minerals or their compositional equivalents through aqueous processing of primary volcanic rocks (Clark et al., submitted manuscript, 2006).

[27] Additional evidence for the mobility of Ni in aqueous solution is evident in analyses of the hematitic spherules at Meridiani. Figure 6 shows a Ni-Fe plot with points representing basaltic soils, hematite-rich soils, and Meridiani outcrop. The soils dominated by hematite spherules and fragments show a clear Ni-Fe correlation with Ni concentrations up to 700 ppm greater than average abraded outcrop analyses. Ni mobilized in solution readily adsorbs onto pre-existing hematite [*Beukes et al.*, 2000] and could be responsible for the elevated Ni in the spherules. Alternatively, during the groundwater recharge events responsible for the development of the hematitic concretions in the model described by *McLennan et al.* [2005], Ni may have been coprecipitated with the iron.

[28] Where did this Ni originate? As shown in Figure 6, the outcrop rocks generally have higher levels of Ni compared to the non-hematitic portion of the overlying sand sheet, but there is no a priori reason to believe that the younger sand unit has any compositional relationship to the basaltic material in the sedimentary rocks. The situation is poorly constrained: The outcrop matrix could have initially had a higher concentration of Ni that diffused into the spherules, or the Ni could have originated from greater depths and precipitated in both the outcrop matrix and the analyzed spherules. The latter option is supported by the observation of lower Ni concentrations in outcrop measurements (Figure 7) where the hematite concretions are smaller and less defined (Figure 8), further suggesting a relationship between Ni content and spherule production. This is consistent with the scenario where the material that formed the outcrop was initially compositionally similar over extensive

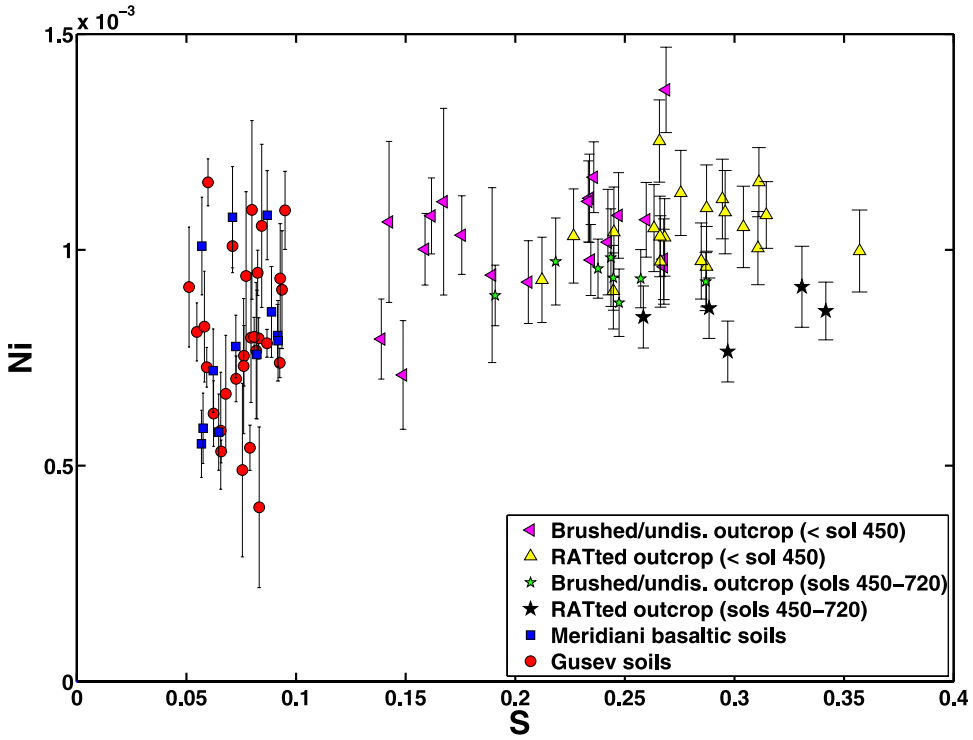

Figure 7. Molar Ni versus S for basaltic soils and Meridiani outcrop. The brushed and undisturbed surfaces of outcrop rocks exhibit lower sulfur levels consistent with soil contamination. Lower Ni concentrations are found in the recent abraded measurements (sols 450–720). Error bars represent 2-sigma precision of the APXS analyses.

lateral scales [*Clark et al.*, 2005], and where Fe and Ni-rich fluids interacted more extensively with sediments in certain regions, perhaps those that were at greater depths.

5. Mixtures

[29] The majority of primary volcanic rocks analyzed on Mars and Martian meteorites studied in terrestrial labs (except the Chassigny dunite), have Ni concentrations less than 330 ppm. Physical mixtures of these rocks cannot achieve the higher levels of Ni observed in targets such as average Mars soil, the outcrops at Meridiani, or the Clovis Class rocks. The possible mafic/ultramafic sequence introduced by *Mittlefehldt et al.* [2006] does indicate that there may be materials in the Martian crust that have inherently high Ni concentrations, but the associated high concentrations of Mg restrict the extent to which physical mixtures of a target such as Comanche can be accommodated in other samples. Table 3 lists a number of mixing constraints for the high Ni Comanche material and generalizes to include other samples. Shown in the table are the maximum quantities of a given component that could be mixed into soils and sedimentary rocks, the element that limits the contribution of that component, and the difference in nickel at the maximum contribution of that component. For example, the abundance of Mg limits the amount of Comanche-like material in average basaltic soil to ~30%. With a composition of 30% Comanche, an additional 200 ppm Ni needs to be added to obtain the level measured in average basaltic soils.

[30] The numbers in Table 3 represent physical mixtures of bulk rock compositions only and do not account for chemical (other than isochemical) weathering that might have occurred after the hypothetical mixing. Given the likelihood of S and Cl condensates from volcanic outgassing, the mobility of Cl and Br [*Yen et al.*, 2005], and their overall volatility, these elements are excluded from this exercise of calculating mixing constraints. Also assumed is a maximum of only two components in the mixture.

5.1. Components of Basaltic Soils

[31] The bright surface dust found at the Martian surface is a globally homogenized unit, and the darker basaltic sands at the two landing sites could also be a global unit or simply a reflection of the similarity in the rocks from which they are derived [*Yen et al.*, 2005; *Morris et al.*, 2006b]. Basaltic compositions clearly dominate the Martian soils and crustal rocks, but the soils cannot be derived from known rock compositions without the addition of nickel.

[32] Table 3 lists the classes of material analyzed thus far that could contribute to the chemical makeup of the soils at Meridiani Planum and in Gusev crater. Of the various groups of rocks that could comprise the soil unit, the Irvine composition allows the greatest percentage contribution to the soils (70%). This value is somewhat suspect, as Irvine was a small target (~10 cm) and was not brushed or abraded prior to analysis. A dust coating indicated by ~2.4 weight percent SO_3 could have artificially skewed this measurement toward the elemental composition of the

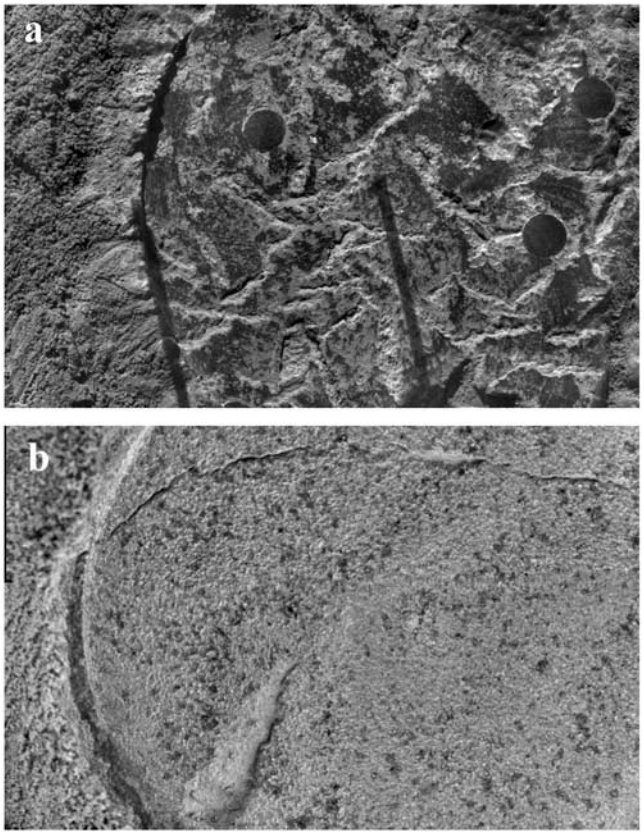

Figure 8. Opportunity MI images of abraded targets, each approximately 4.5 cm by 3 cm. (a) "Guadalupe" (sol 35) showing partially abraded spherules. (b) "Ted" (sol 691; mosaic of 4 images) with no clear evidence of hematitic spherules, one of several indicators of distinct changes in outcrop rocks along the traverse.

soils. Nonetheless, approximately 300 ppm of additional Ni is still required to produce the Ni levels in the soils. In fact, not even Comanche with 1000 ppm Ni can, by itself, add enough Ni to account for the concentration in the soils, because the addition of Comanche to the soils is limited to 30% by the abundance of Mg.

[33] An excess of Ni in the soils is also apparent from a plot of this element versus the percentage of olivine from candidate source rocks for the soil (Figure 9). During crystallization from a magma, Ni^{2+} partitions strongly into olivine, as indicated by the roughly linear relationship for the Martian meteorites. Adirondack and Wishstone class rocks plot within the field of Martian meteorites, while soil samples have much more Ni than indicated by the plotted Ni-Ol trend line.

[34] It is therefore reasonable to hypothesize that a few percent meteoritic material is necessary to account for the Ni in the soils, with the caveat that the origin of the global soil unit is not yet fully understood. There could be a high-Ni source with a soil-like composition (different from all the primary rocks analyzed, including the Martian meteorites available here on Earth) or a process for weathering and concentrating Ni in surface fines, such as preferential alteration of olivine [*Newsom et al.*, 2005]. Perhaps there was a process whereby a Ni-rich target like Comanche could be responsible for the Ni content of the soils but chemical weathering removed the excess Mg, Fe, and Cr (see section 6.1). While these ad hoc alteration processes cannot be ruled out with the available data, they do seem unlikely given the relatively unweathered nature of the Martian soils, especially the dark sands where the Fe-mineralogy is dominated by olivine.

[35] An interesting exercise is to consider the composition of other material in the solar system that could potentially contribute to Martian soils. The average solar abundance is useful for providing certain constraints; however, given Mars' proximity to the asteroid belt and the likelihood that dust and sand grains generated there spiral inward toward the sun [*Rietmeijer*, 1998] to be swept up by the Martian gravity well, it makes sense to consider an influx with the composition of average interplanetary dust particles (IDP). Many IDPs are chondritic in composition, but they are very heterogeneous. To first order they have compositions that cluster around that of CI chondrites [*Rietmeijer*, 1998]. Thus the discussion above regarding chondritic mixing in Mars soils applies to IDPs as well.

[36] The enhanced abundances of siderophile elements in lunar soils and breccias, and in howardites, polymict breccias likely from 4 Vesta, are best matched as being derived from CM chondrite debris [*Chou et al.*, 1976; *Wasson et al.*, 1975]. This led to the conclusion that CM chondrites have been the most common type of debris in the inner solar system for the last ~4 Gyr [e.g., *Chou et al.*, 1976]. Clasts of CM chondrites are the most commonly observed meteoritic debris in vestan breccias [*Zolensky et al.*, 1996] in accord with the siderophile element evidence [*Chou et al.*, 1976]. In addition, a CM fragment was found in an Apollo

Table 3. Mixing Constraints[a]

	Maximum Contribution – Limiting Element – Ni Deficiency			
Component	Basaltic Soils	Meridiani Outcrop	Clovis Class	Home Plate
Adirondack Class	60% – Cr – 400 ppm	30% – Cr – 600 ppm	30% – Cr – 550 ppm	80% – Ca – 200 ppm
Wishstone/Watchtower	15% – P – 500 ppm	20% – P – 600 ppm	20% – P – 600 ppm	20% – P – 300 ppm
Backstay	45% – K – 400 ppm	45% – Al – 550 ppm	35% – K – 550 ppm	30% – K – 250 ppm
Irvine	70% – Mg – 300 ppm	75% – Na,Al – 400 ppm	50% – K – 450 ppm	45% – K – 200 ppm
Bounce rock	55% – Ca – 450 ppm	40% – Ca – 600 ppm	40% – Ca – 550 ppm	50% – Ca – 300 ppm
Comanche	30% – Mg – 200 ppm	30% – Mg – 350 ppm	20% – Cr – 400 ppm	35% – Ni – 0
Basaltic soil	–	60% – Na, Al – 350 ppm	35% – Zn – 400 ppm	65% – Ni – 0
CI	4.7% – Ni – 0	5.9% – Ni – 0	5.6% – Ni – 0	3.1% – Ni – 0
Barberton	30% – Ni – 0	35% – Ni – 0	35% – Ni – 0	20% – Ni – 0

[a]The maximum amount of the component in the left column, the limiting element, and the amount of additional Ni necessary to make up the difference is calculated for 4 groups of samples.

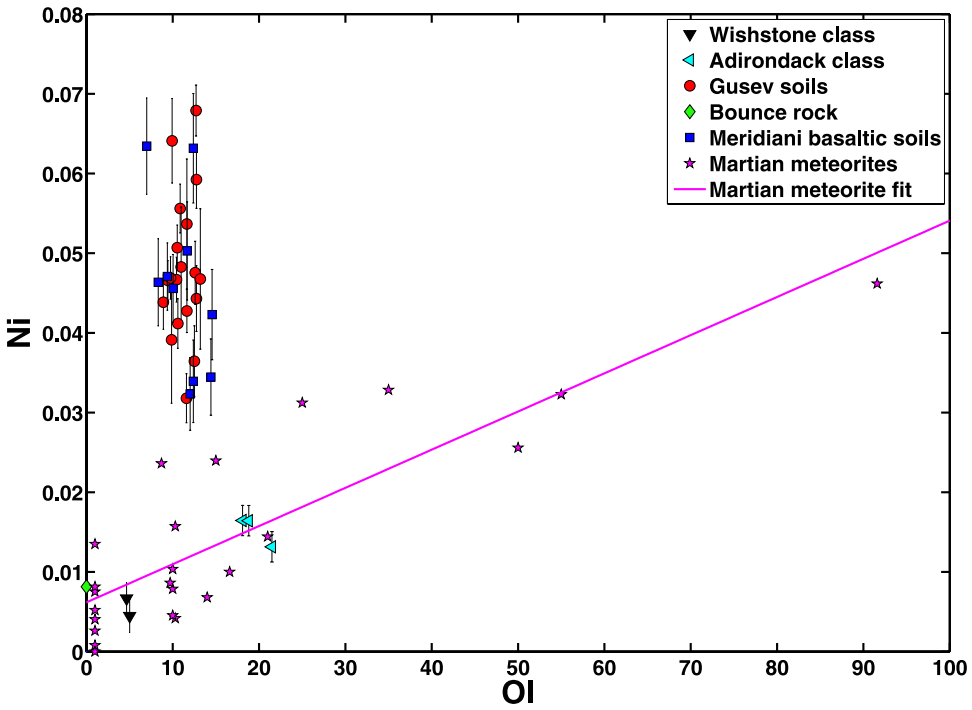

Figure 9. Ni versus percent olivine. Martian meteorite data from *Meyer* [2003]; "small" olivine abundances are plotted as 1%. Olivine abundances for MER samples obtained from the Mössbauer spectrometer [*Morris et al.*, 2006a; 2006b] adjusted for iron content and assuming Fo 50 composition [*McSween et al.*, 2006a]. Error bars represent 2-sigma precision of the APXS analyses.

12 regolith sample [*Zolensky et al.*, 1996]. However, compared to the differences between Mars surface rocks and CI chondrites, CM chondrites are insignificantly different from the latter. CM chondrites show slight depletions in volatile and moderately volatile elements, thus Na, S, Cl, K, Zn and Br are depleted in CM chondrites compared to CI, but by factors of <2. As is the case for CI chondrites, enhanced Ni is the most significant result of small amounts of CM chondrite debris in Mars soil.

5.2. Components of Meridiani Outcrop

[37] The Late Noachian to Early Hesperian layered outcrop at Meridiani consists of a mixture of sulfate and silicate sediments [*Squyres and Knoll*, 2005] that experienced multiple stages of diagenesis resulting from episodes of groundwater exposure [*McLennan et al.*, 2005; *Grotzinger et al.*, 2005]. The Ni levels in the outcrop average approximately 630 ppm, which is significantly higher than can be reproduced by mixtures with known materials from Mars (Table 3). The collection of known Martian meteorites also has insufficient quantities of Ni to account for the composition of the Meridiani rocks.

[38] Options for accounting for the Ni content of the outcrop include the following: (1) The silicate portion of the rocks are derived from yet-unidentified Ni-rich materials, (2) the groundwater which infiltrated the sediments carried Ni ions in solution which deposited in the outcrop matrix, possibly as an adsorbate on, or coprecipitate with, the fine grained hematite and/or were incorporated directly into sulfate minerals, or (3) influx of meteoritic Ni occurred when the sand sheet and dunes lithified in the outcrop were active. If the excess Ni in Meridiani outcrop relative to average Martian meteorites resulted entirely from meteoritic influx, as much as 6% of a CI composition would need to be added [*McLennan et al.*, 2005].

[39] Thus far, there is no clear evidence for an appropriate high-Ni source region for the silicate sediments. As pointed out above, the Ni content of the Martian meteorites, apart from the Chassigny dunite are low, as are the basaltic rocks analyzed by both MER rovers. On the other hand, by the broader standards of basaltic volcanism throughout the solar system, basaltic Ni contents in excess of 500 ppm are by no means unusual [*Basaltic Volcanism Study Project*, 1981]. The Comanche deposits on the other side of the planet exhibit sufficient levels of Ni, but are limited in the extent of mixing because of high levels of Mg (Table 3). Addition of Comanche-like material followed by redistribution of elements through aqueous processing is possible, though there are few constraints to test this hypothesis. The data showing the increase in Ni in the hematite spherules establish the idea that this element moved with the groundwater (section 4.4). The down-section trend in Endurance crater exhibits a gradual decrease in Ni levels in abraded rocks, suggesting a possible correlation with the water-related Mg-sulfates [*Clark et al.*, 2005]. Thus there may be mechanisms for Ni enhancements in these rocks that do not necessarily involve the addition of chondritic material.

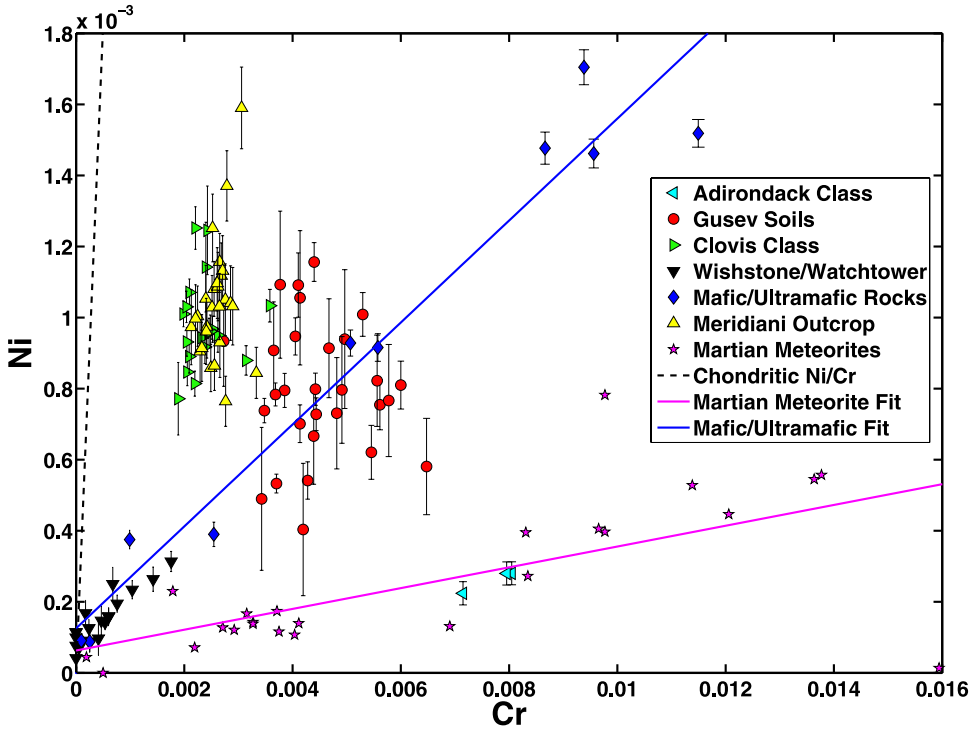

Figure 10. Molar plot of nickel versus chromium for various classes of material. Two families of volcanic rocks, each with a characteristic Ni:Cr ratio, are evident. Meridiani outcrop and Clovis class rocks plot above the blue and magenta trend lines, suggesting either fundamentally different source materials or the addition of meteoritic nickel. Error bars represent 2-sigma precision of the APXS analyses.

5.3. Other Classes of Material at Gusev Crater

[40] Clovis class rocks in the Columbia Hills are massive to layered clastic and poorly sorted rocks with a bulk basaltic composition [*Squyres et al.*, 2006]. Mössbauer observations showing that up to 40% of the iron is in the form of goethite (α-FeOOH) indicate that this class of rocks has been aqueously altered [*Morris et al.*, 2006a]. The elevated Ni concentrations in these rocks, averaging approximately 600 ppm, is not a product of simple mixing with any of the other known groups of Martian samples (Table 3) including the Martian meteorites. An external contribution of Ni is likely. However, given the role of water in the development of goethite in these rocks, the possibility of aqueous redistribution of the elemental constituents, including concentration of Ni in these rocks, cannot be ruled out.

[41] Home Plate is a light-toned, approximately circular feature ~80 meters in diameter which is visible from orbit. Analyses by Spirit instruments indicate that it consists of partially weathered layered rocks of basaltic composition. In contrast to the deposits at Clovis, the Ni concentration at Home Plate is substantially lower, approximately 330 ppm. Ni concentrations at these levels are consistent with primary volcanic material analyzed on Mars (Adirondack-class basalts) and the higher-Ni Martian meteorites, without the need for a chondritic addition.

[42] The Peace Class materials are magnetite-rich sandstones of dominantly olivine and pyroxene grains cemented by sulfates [*Squyres et al.*, 2006]. When the sulfate component is removed from the Peace composition, the chemistry is similar to the high-Ni Comanche rocks of the mafic-ultramafic sequence described in section 4.3. Given this apparent genetic relationship, it is unlikely that the elevated Ni concentrations in Peace class rocks are result from addition of a meteoritic component.

[43] The Paso Robles Class deposits dominated by hydrated ferric sulfates have highly variable minor and trace element signatures. Ni concentrations in these samples range from ~100 to ~900 ppm and likely result from aqueous processes at low water to rock ratios. The details of the Paso Robles Class of materials are discussed by *Ming et al.* [2006] and *Morris et al.* [2006a].

6. Elemental Relationships

[44] Plotting elemental trends through related samples can help illustrate the overall chemical variability in the analyzed samples and provide insight into possible mixing relationships with chondritic material. Ni-Cr, Ni-Mg, and Ni-Ti relationships, for example, are useful in establishing families of volcanic rocks, and identifying classes of materials that likely had different evolutionary histories. In addition, plots of S-Cl can help establish limits on the amount of meteoritic sulfur.

6.1. Nickel Versus Chromium

[45] Ni and Cr are compatible elements in most mafic-ultramafic liquids and tend to behave similarly during

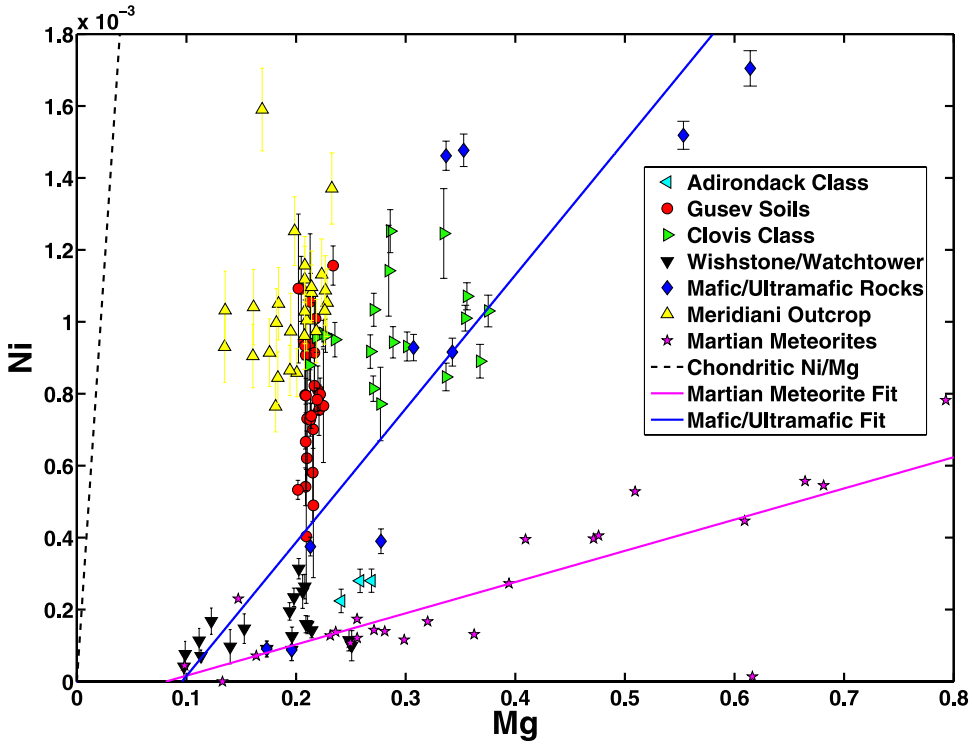

Figure 11. Molar plot of nickel versus magnesium for various classes of material. Trends of the mafic/ultramafic sequence and the Martian meteorites are similar to those shown in the Ni:Cr plot (Figure 10), suggesting that igneous processes dominate. Error bars represent 2-sigma precision of the APXS analyses.

crystallization. Figure 10 shows that the Ni:Cr of Gusev plains basalts (Adirondack class) fit well within the field of Martian meteorites, consistent with the relationship described by *McSween et al.* [2006a]. The data points from the mafic-ultramafic sequence described in section 4.3 define a different line that may represent an older family of volcanics with several samples highly enriched in Ni. The slope of the Ni-Cr trend in these ancient rocks is much shallower than the chondritic ratio, indicating that the elevated Ni and Cr do not likely result from meteoritic contamination. Thus there are two families of Martian rocks that can contribute material with fixed Ni-Cr ratios to Martian soils and sedimentary rocks.

[46] The groupings for Clovis class [*Squyres et al.*, 2006] and the abraded Meridiani outcrop rocks, however, are offset from these two sets of volcanic rocks. Several options for explaining these discrepancies are possible: (1) The components of these fine-grained sedimentary rock classes are unrelated to the two identified families of volcanic rocks and have inherently different Ni-Cr ratios, and/or (2) aqueous processes redistributed Ni and Cr to the observed levels in Clovis and Meridiani outcrop rocks, and/or (3) meteoritic infall enhanced the Ni concentration in the sedimentary rocks. The first possibility cannot reasonably be assessed, as it is difficult to include or exclude components of unknown materials. The second option is possible, especially given that both of these rock classes have experienced aqueous processing. However, the scatter in the majority of the data (yellow and green points in Figure 10) appears to parallel the Ni-Cr trend line for a mixture with chondritic material. If the offset of Ni:Cr in Clovis and Meridiani outcrop rocks above the magenta (Martian meteorites) and blue (mafic/ultramafic sequence) lines resulted from a meteoritic addition of Ni, the addition of 5.0 to 3.3% chondritic material, respectively, would be indicated.

[47] Section 5.1 addresses the likely contribution of meteoritic material to Martian soils, which is further highlighted in the Ni:Cr plot shown in Figure 10. The Gusev soil data points exhibit Ni enhancements relative to the family of volcanics indicated by the Martian meteorites and straddles the trend line established by the mafic/ultramafic sequence of rocks. From Microscopic Imager images, it is evident that the soil analyses with lower Ni concentrations tend to have a greater abundance of rock fragments, consistent with mixing with Adirondack class basalts. Many soil data points exhibit statistically significant excesses of Ni above even the high-Ni mafic/ultramafic sequence of rocks. On the basis of Ni-Cr ratios, the meteoritic component of the soils is up to 2.3% if the "base" Ni-Cr value is defined by the mafic/ultramafic sequence of rocks or an average of approximately 3.3% if the "base" Ni-Cr value stems from the Martian meteorites and Adirondack class basalts.

[48] Counterparts to the Ni-Cr plot are Ni-Mg (Figure 11) and Ni-Ti (Figure 12). If igneous processes dominate, Ni-Mg should mimic Ni-Cr, and Ni-Ti should show a trend opposite to that of Ni-Cr. This is, in fact, generally the case for the fits defined by the Martian meteorites and the mafic/

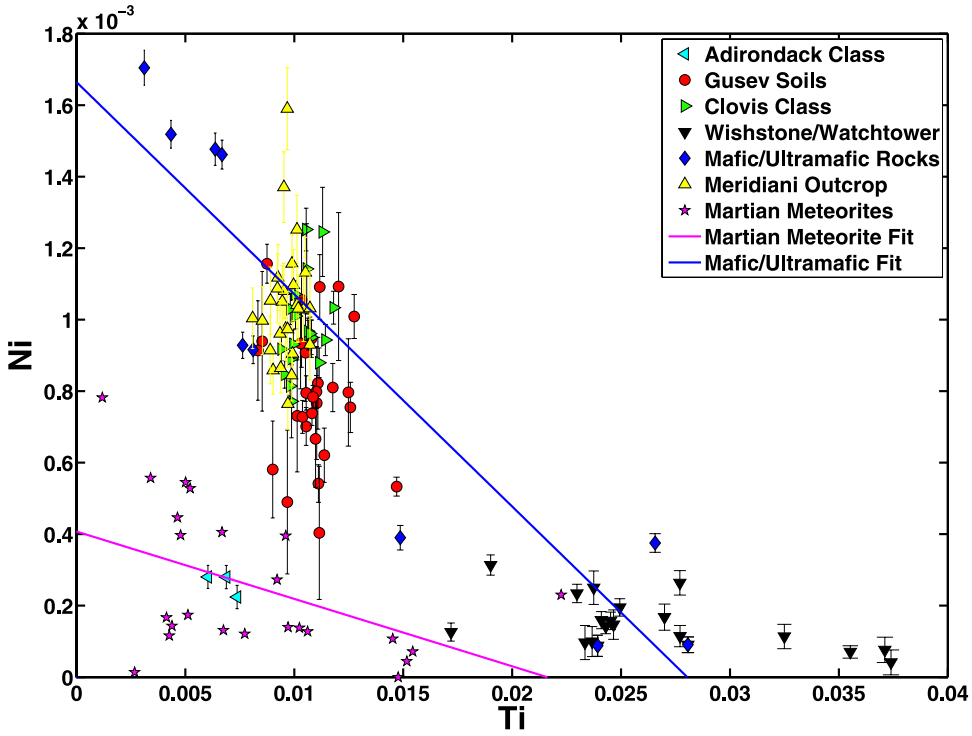

Figure 12. Molar plot of nickel versus titanium for various classes of material. Trends in the blue and magenta lines are opposite of those in Figures 10 and 11. The chondritic Ni:Ti ratio lies essentially along the y-axis of this plot. Error bars represent 2-sigma precision of the APXS analyses.

ultramafic sequence of rocks. In the Ni-Mg plot, the points for Clovis class and Meridiani outcrop rocks are shifted to the right relative to their positions on the Ni-Cr plot suggesting that Mg has been redistributed by weathering processes. This inference is consistent with the likelihood of Mg-sulfates in Meridiani rocks [*Clark et al.*, 2005] and aqueous alteration of Clovis rocks [*Ming et al.*, 2006; *Morris et al.*, 2006a]. Figure 11 also shows that the Ni concentration in Gusev soils is independent of the Mg abundance and roughly parallels the Ni-Mg ratio of chondritic material.

6.2. Sulfur

[49] Sulfur is another element that is abundant in meteoritic material. Unfortunately, it is also a major element in Martian samples with clear evidence that it is geochemically mobile. The decrease in Mg-sulfate with depth in Endurance crater [*Clark et al.*, 2005], the concentration of Mg- and Ca-sulfate cements in Peace class rocks [*Squyres et al.*, 2006; *Ming et al.*, 2006], and the significant enhancements in sulfur in certain subsurface soil samples [*Haskin et al.*, 2005] all indicate secondary redistribution of S. This transport complicates attempts to estimate the magnitude of meteoritic input on the basis of sulfur.

[50] There is, however, one perspective on S that provides a possible constraint. Figure 13 presents a molar plot of S versus Cl for basaltic soils at Gusev and Meridiani. The linear relationship is a global attribute that may represent the addition of condensates of volcanic exhalations [*Clark and van Hart*, 1981]. The fit through these points should go through the origin if the soil simply contained variable amounts of the volcanic emissions and if neither chemical reprocessing of the deposits nor addition of S or Cl has occurred. The least squares fit in Figure 13 intercepts the y-axis slightly above the origin, indicating a possible addition of up to 4.5% meteoritic sulfur to the Martian surface soil unit.

[51] Another approach to looking at S relationships with meteoritic material is based on the Ni versus S plot shown in Figure 7. Higher concentrations of sulfur in this set of Meridiani data are generally found in the abraded and "clean" interiors of analyzed outcrop. Undisturbed and lightly brushed outcrop rocks have lower sulfur contents, consistent with contamination from dust and basaltic sand, which have even lower sulfur levels. The interesting aspect of Figure 7 is in the locations of data points (plotted as stars) for outcrop samples that were analyzed outside of Eagle and Endurance craters. These data points still display a similar behavior in the S content of undisturbed/brushed versus abraded targets, but the nickel content of these measurements is systematically lower.

[52] One potential explanation for the higher Ni contents of rocks within craters is that they are more contaminated by projectile material. Depth-to-diameter ratios suggest that both Eagle and Endurance craters are primary impacts [*Grant et al.*, 2006]. Impact simulation models indicate that a major portion of the projectile coats the floor and walls of the crater after the impact for near-vertical impacts, but projectile material is increasingly dispersed outside the crater as impact angle decreases [*Pierazzo and Melosh*, 2000]. The most probable impact angle, however, is 45° and thus systematic difference in Ni inside versus outside craters at Meridiani is not likely. Terrestrial experience is

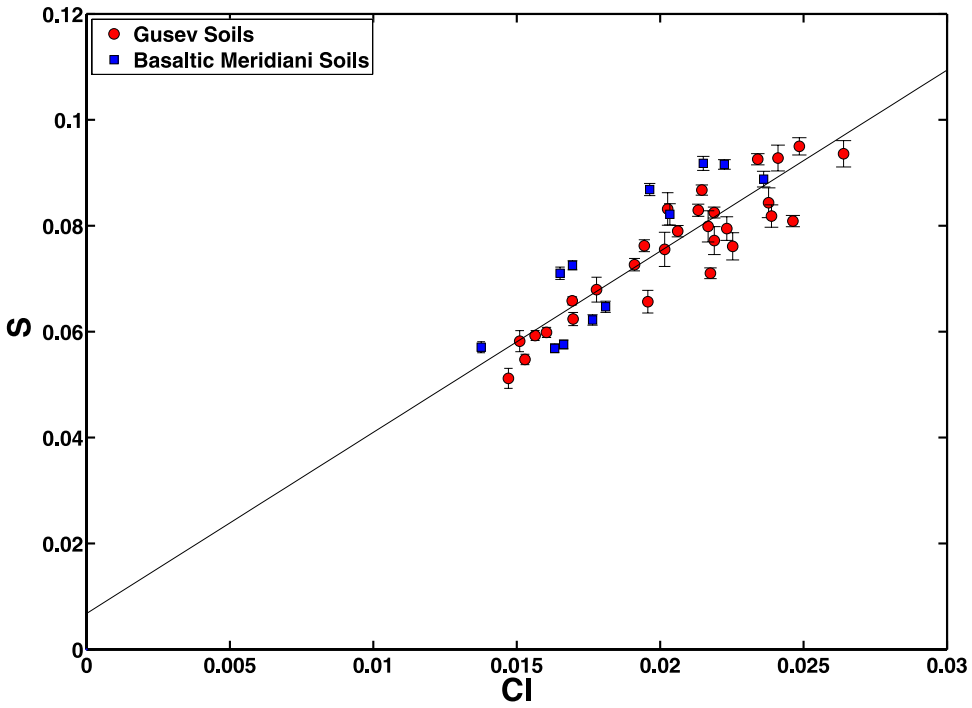

Figure 13. Molar S versus Cl and least squares fit for basaltic soils. Error bars represent 2-sigma precision of the APXS analyses.

severely limited because most craters are old and degraded; compositional evidence from the crater walls has been eliminated. At Meteor Crater, analyses of target rock from a systematic stratigraphic section collected from within the crater [*Mittlefehldt et al.*, 2005] did not find evidence for projectile contamination. The highest Ni content is equivalent to 0.05% projectile material, but this plausibly represents the natural fluctuation in Ni in the target rock. An alternate explanation for the lower nickel content of Meridiani outcrop analyses outside craters is that it is unrelated to meteoritic contributions, but is associated with changes in the aqueous conditions under which the concretions formed (section 4.4).

7. Magnetic Properties of the Dust

[53] An additional perspective on possible meteoritic material in Martian samples is provided by the magnetic properties investigation. Each rover has of a suite of Sm_2Co_{17} magnets to collect airborne dust (sweep, capture, and filter magnets) and magnetic particles in tailings generated by the rock abrader (RAT magnets) [*Madsen et al.*, 2003]. The sweep magnet is a small ring magnet designed with a field strength sufficiently large that only particles with a specific susceptibility less than 30×10^{-8} m^3/kg can enter the 4 mm diameter central region [*Madsen et al.*, 2003]. Pancam imaging of this magnet (Figure 14) has shown that the central portion has remained essentially free of dust, indicating that nearly all Martian dust has an appreciable magnetic susceptibility [*Bertelsen et al.*, 2004].

[54] The capture magnet is a 45 mm diameter magnet designed to capture airborne dust for analyses by the in-situ instruments. Mössbauer analyses of the collected dust indicate the presence of the basaltic components seen by this instrument in typical soils: Olivine, pyroxene, nanophase ferric oxide(s), and magnetite, but at different relative concentrations [*Goetz et al.*, 2005]. APXS analyses of the collected dust show that a major portion of the iron-containing material on the capture magnet is associated with Ti and Cr (Gellert et al., manuscript in preparation, 2006), consistent with titanomagnetite and possibly chro-

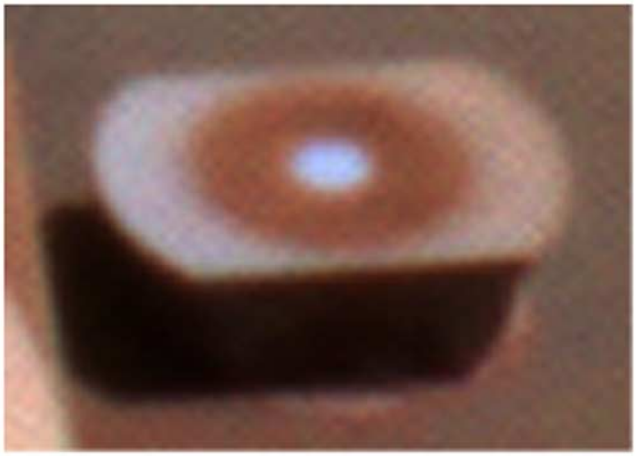

Figure 14. False color image of Spirit sweep magnet imaged by Pancam (sol 837). Central portion (above the strong ring magnet) remains mostly clear of atmospheric dust, indicating a significant level of magnetic susceptibility for nearly all airborne dust grains.

Table 4. Meteoritic Contribution From the Impact Crater Record

	Bin 1	Bin 2	Bin 3	Bin 4	Bin 5	Bin 6	Bin 7	Bin 8	Sum, mm
Crater diameter, km	1.0	1.4	2.0	2.8	4.0	5.7	8.0	11.3	
Projectile diameter, m	31	48	74	115	179	277	430	667	
Number per square km									
Late/Mid Amazonian	1.1E − 04	5.6E − 05	2.8E − 05	1.4E − 05	-	-	-	-	
Mid/Early Amazonian	4.2E − 04	2.1E − 04	1.1E − 04	5.3E − 05	-	-	-	-	
Amazonian/Hesperian	1.1E − 03	5.6E − 04	2.8E − 04	1.4E − 04	-	-	-	-	
Late/Early Hesperian	2.3E − 03	1.1E − 03	5.6E − 04	2.8E − 04	1.4E − 04	7.0E − 05	3.5E − 05	1.8E − 05	
Hesperian/Noachian	3.4E − 03	1.7E − 03	8.5E − 04	4.2E − 04	2.1E − 04	1.1E − 04	5.3E − 05	2.6E − 05	
Late/Mid Noachian	-	-	-	-	1.1E − 03	5.7E − 04	2.8E − 04	1.4E − 04	
Mid/Early Noachian	-	-	-	-	2.3E − 03	1.1E − 03	5.7E − 04	2.8E − 04	
Thickness, mm									
Late/Mid Amazonian	1.7E − 03	3.1E − 03	5.8E − 03	1.1E − 02	-	-	-	-	0.02
Mid/Early Amazonian	6.3E − 03	1.2E − 02	2.2E − 02	4.1E − 02	-	-	-	-	0.08
Amazonian/Hesperian	1.7E − 02	3.1E − 02	5.8E − 02	1.1E − 01	-	-	-	-	0.2
Late/Early Hesperian	3.3E − 02	6.2E − 02	1.2E − 01	2.2E − 01	4.0E − 01	7.5E − 01	1.4E + 00	2.6E + 00	5.6
Hesperian/Noachian	5.0E − 02	9.3E − 02	1.7E − 01	3.2E − 01	6.1E − 01	1.1E + 00	2.1E + 00	3.9E + 00	8.4
Late/Mid Noachian	-	-	-	-	3.2E + 00	6.0E + 00	1.1E + 01	2.1E + 01	42
Mid/Early Noachian	-	-	-	-	6.5E + 00	1.2E + 01	2.3E + 01	4.2E + 01	83

mite. The association with Ti suggests that physical weathering of basaltic materials, rather then chemical processes that would tend to produce a more pure magnetite precipitate, may play a significant role in generating the magnetic fines [*Coey et al.*, 1990; *Morris et al.*, 1990, 2001a; *Madsen et al.*, 1995].

[55] How is it possible, however, that all of the dust has some level of magnetic susceptibility and yet they are physical weathering products of basaltic rocks? If an arbitrary Martian rock is crushed by impact into micron-sized dust grains [e.g., *Pollack et al.*, 1979; *Lemmon et al.*, 2004], how does each individual grain retain characteristics of a magnetic phase? The olivine in typical basaltic soils is Fo40 to Fo60 in composition [*McSween et al.*, 2006a], but chemical zoning is likely. A portion of the olivine will be Mg-rich with a low magnetic susceptibility, and should penetrate to the center of the sweep magnet (magnetic susceptibility of pure forsterite is -0.39×10^{-8} m^3/kg) [*Hunt et al.*, 1995]. Furthermore, the typical grain sizes in the Martian meteorites is a few hundred microns, so a random sampling of micron sized regions should yield low-susceptibility minerals such as plagioclase and quartz. The reason the center of the sweep magnet stays clean is likely because the dust grains are composite particles [*Hargraves et al.*, 1977; *Hviid et al.*, 1997], each with a (titano)magnetite component [*Goetz et al.*, 2005].

[56] The generation of such composite particles may involve secondary alteration processes including dissolution, oxidation, and precipitation of ferrimagnetic phases [*Arlauckas et al.*, 2006] and/or the development of coatings of high-susceptibility nanophase ferric oxide (npOx) particles [e.g., *Morris et al.*, 1989]. Another possible mechanism for producing composite grains with magnetite is related to meteoritic contributions to the surface. Micrometeorites analyzed in terrestrial laboratories exhibit magnetite rinds formed as a result of heating during atmospheric entry [*Genge and Grady*, 1998]. Similar examples of surficial magnetite are present on interplanetary dust particles [*Bradley et al.*, 1996]. Entry vaporization and recondensation of metallic vapors produce metal oxides in Earth's atmosphere [*Rietmeijer*, 2000], and similar processes are expected for Mars [*Pesnell and Grebowsky*, 2000]. Experimental evidence suggests that the impact of larger objects under a CO_2 atmosphere may also produce magnetite during crystallization of the impact melts [*Morris et al.*, 2001b]. Taken collectively, these results suggest that at least a portion of the Martian dust could be a product of meteoritic material processed by entry heating, or possibly a product of impact vaporization/melting and recondensation resulting from larger impacts [e.g., *Wdowiak et al.*, 2001].

8. Cratering Record

[57] In addition to the constraints based on Ni abundances, an estimate of the lower limit on the quantity of meteoritic material at the Martian surface can be calculated using the impact cratering record. Such a calculation also provides a consistency check of the concentrations determined from MER APXS data. Studies of the landing sites indicate that the Gusev plains are Late Hesperian in age while the layered outcrop at Meridiani are Late Noachian with an overlying Late Amazonian sand sheet (see discussion and references of *Golombek et al.* [2006a]). Working backward from these ages, the crater population in $(2)^{1/2}$ intervals is calculated using equations of *Hartmann* [2005] and summarized in Table 4. We can then calculate the amount of meteoritic material that corresponds to the observed crater population.

[58] The projectile size for a given crater diameter is estimated using scaling relationships from *Melosh* [1989]: The apparent diameter (D_{at}) of the transient crater can be represented in terms of the projectile density (ρ_p), the target density (ρ_t), gravity (g), the projectile diameter (L), and the impact kinetic energy (W) as follows:

$$D_{at} = 1.8\ \rho_p^{0.11}\ \rho_t^{-1/3}\ g^{-0.22}\ L^{0.13}\ W^{0.22}$$

where all values are in MKS units. For this first-order approximation, it is reasonable to assume that $\rho \sim \rho_p \sim \rho_t$. Using a transient crater diameter equal to 84% of the diameter of the final simple crater [*Melosh*, 1989], representing W in terms of ρ, L, and V (impact velocity), and

rearranging produces the following relationship between the observed crater diameter (D) and the projectile diameter:

$$L = 0.58\ D^{1.27}\ g^{0.28}\ V^{-0.56}$$

Impact velocities will vary depending upon the orbital parameters of the object and will range from ~5.6 km/s for material in nearby orbits to ~31 km/s for long period comets [*Carr*, 1984]. The projectile diameters listed in Table 4 assume an intermediate impact velocity of 10 km/s, representative of asteroids and short period comets [*Carr*, 1984].

[59] Using the projectile diameters and the numbers of impacts for each crater size range, the thickness of meteoritic material, if evenly spread over the surface of Mars, is calculated and summarized in Table 4. These results indicate that the impacts associated with the Late Hesperian surface age at Gusev Crater contributed meteoritic material equivalent to a global layer approximately 5.6 mm thick. The corresponding calculation at Meridiani Planum suggests 42 mm of accumulated meteoritic material after emplacement of the layered sediments in the Late Noachian. This value could be an overestimate as Hesperian aged materials are apparently absent from the geologic record at Meridiani [*Golombek et al.*, 2006a]. On the other hand, in the older eras, larger diameter craters (not included in the calculation) become more important and could add significantly to the accumulation of meteoritic material. Nonetheless, this calculation provides a rough estimate of meteoritic accumulations since the Late Noachian.

[60] Hydrodynamic modeling shows that tracer particles representing the projectile end up primarily along the walls of the crater for near-vertical (60° to 90°) impacts, while most of the projectile is ejected from the crater for impact angles less than 30° [*Pierazzo and Melosh*, 2000]. Thus, even though the impact gardening depth is on the scale of the crater (~kilometers), the majority of the projectile ends up at or near the immediate surface after distribution by the impact plume. If the ~tens of millimeters of meteoritic material calculated above were spread through a depth of a few meters through aeolian transport or further impact gardening, the average quantity of meteoritic material in this layer would be approximately 1%.

9. Synthesis

[61] Assuming a chondritic composition for the meteoritic flux to the Martian surface, the nickel content of basaltic soils, the Meridiani outcrop rocks, and the Clovis class material establishes an absolute upper limit of 6.5% meteoritic debris in these units. This value assumes that all of the Ni in these fine-grained sediments is exogenic, which is certainly not correct. Tighter constraints on the upper limit are derived from relationships between Ni and Cr (section 6.1) and between S and Cl (section 6.2). These trends indicate an upper limit of 4.5% meteoritic material in basaltic soils on the basis of sulfur and upper limits in the 3.3% to 5.0% range based on nickel for Meridiani outcrop and Clovis class material, depending upon assumptions on the source rocks. These values also represent fairly conservative upper limits. Given the mobility of Ni in solution, which may have enhanced the Ni concentrations in Meridiani outcrop rocks and possibly Clovis class rocks as well, and given indications that ancient volcanics may have been more Ni-rich, we believe that an upper limit of 3% fine-grained meteoritic debris in basaltic soils, Meridiani outcrop rocks, and Clovis class materials is reasonable.

[62] On the other end of the scale, it is clear that the Ni levels in basaltic soils, Meridiani outcrop rocks, and Clovis class materials cannot be achieved by simple addition of other Martian materials of known compositions. In such mixtures, elemental constraints are violated. Aqueous processes may have acted to remove and concentrate various elements to achieve the Ni-levels in these units from the addition of Ni-rich Martian rocks, but the addition of a small meteoritic component provides a simpler explanation.

[63] As established in section 8, the presence of impact craters can set an approximate lower limit of ~1% on the incorporation of meteoritic material. The meteoritic contribution from the ongoing influx of interplanetary dust particles is comparable in magnitude to material delivered by objects large enough to form craters. Using an intermediate value of 10^7 kg/yr in the estimate of IDP flux calculated by *Flynn and McKay* [1990], a ~30 mm thick global layer is produced every 10^9 years, which also corresponds to a ~1% concentration of meteoritic material.

[64] In each of these estimates, it is assumed that the vertical mixing depth is on the order of several meters. This is consistent with the ~1 meter thickness of the Meridiani sand sheet [*Soderblom et al.*, 2004] and the ~10 meters of impact regolith on the Gusev plains [*Golombek et al.*, 2006b]. Attempts to establish soil production rates or to provide higher fidelity estimates in these calculations are complicated by the apparent loss of the Hesperian aged surfaces at Meridiani and the removal of soil from the Gusev site under the current wind regime [*Greeley et al.*, 2006]. Nonetheless, it is clear that percent-level meteoritic contributions from IDPs and larger impactors are reasonable lower limits.

[65] Thus a number of lines of evidence suggest that a range of 1% to 3% chondritic influx, corresponding to roughly 100 to 300 ppm Ni, is consistent with the elemental chemistry of Martian surface materials. Although meteoritic accumulation processes differ between the moon and Mars, with aeolian distribution likely dominant for fine grained meteoritic debris on Mars, this range for the estimate of the meteoritic contribution to the Martian surface is consistent with the measured value of 1.5% to 2% CI material on the lunar surface [*Taylor*, 1982].

[66] An additional exercise to consider is the accumulation time required to produce the Ni levels observed in the APXS data. Using the full range of IDP fluxes calculated by *Flynn and McKay* [1990], it takes between 50 Ma and 1 Ga to produce each 100 ppm of meteoritic Ni. An intermediate value of ~100 Ma per 100 ppm of Ni is roughly consistent with the cratering age of the Meridiani sand sheet (~400 Ma) and the several hundred ppm of Ni in this unit that is likely to be meteoritic. Interestingly, this Late Amazonian deposit has Ni levels comparable to the Late Noachian (~3.7 Ga) rocks at Meridiani and the Clovis class rocks exposed at the Late Hesperian surface (~3.5 Ga) within Gusev Crater (Table 2). Given that the absolute ages of these rocks should be independent of the time it took to

accumulate the sediments that produced them, it is reasonable that the Ni concentrations measured in these rocks do not correspond to their ages. The amount of meteoritic material that should have accumulated *above* these rocks, however, should be related to their ages. Unfortunately, the apparent loss of the Hesperian surface at Meridiani [*Golombek et al.*, 2006a] and the deflationary environment at Gusev Crater [*Greeley et al.*, 2006] may have removed meteoritic accumulations from areas accessed by the rovers.

10. Meteoritic Carbon

[67] Assuming an influx of meteoritic material with an average composition equivalent to CI chondrites, the addition to the Martian environment of other important elements, such as carbon, can be estimated. The solar abundance of carbon is approximately 3.3 times greater than the quantity of nickel [*Lodders*, 2003]. The upper range of Ni detected in typical MER samples is ~700 ppm, and if all of this were meteoritic, ~2300 ppm C would be associated with this influx. However, it is unrealistic to expect that all the Ni measured by the rovers is exogenic. As discussed above, a reasonable range for meteoritic Ni is 100 to 300 ppm, suggesting an associated 330 to 990 ppm C delivered to Mars through meteoritic influx.

[68] Using measurements of interplanetary dust particle (IDP) flux at Earth applied to Mars, *Flynn* [1996] estimates a current accretion rate of 2.4×10^5 kg/yr of unaltered carbon at the Martian surface. Applied over the ~3.5 and >3.7 Ga cratering ages of the Gusev plains and the Meridiani outcrop [*Golombek et al.*, 2006a], respectively, a global layer of organic carbon ~2 mm thick is predicted. This should be a conservative lower limit given that ancient flux rates were substantially higher than those at present [*Flynn*, 1996]. Mixing through an active aeolian regime several meters in thickness would result in dilution to the ~400 ppm level. This value is entirely consistent with the amount of meteoritic carbon implied by the measured Ni concentrations. It is expected to be on the lower end of the 330 to 990 ppm range because Ni that enters the Martian atmosphere, even if vaporized, eventually settles to the surface, whereas organic molecules can volatilize into CO_2 and other gases during entry heating and remain in the atmosphere.

[69] The absence of detectable organic compounds [*Biemann et al.*, 1977] at levels three or four orders of magnitude lower than what is predicted to be there from meteoritic input alone is a clear indicator of surface or atmospheric processes that have destroyed organic compounds [e.g., *Yen et al.*, 2000]. Future missions [*Mahaffy and the SAM Science Team*, 2005; *Bada et al.*, 2005] may achieve lower organic detection limits than the 1976 Viking Lander instrumentation, access organics in rock interiors which are protected from oxidizing species, or be able to attain temperatures capable of pyrolyzing and detecting photodegraded organics [*Benner et al.*, 2000].

11. Conclusions

[70] 1. Measurements of nickel in Martian samples provides an excellent tracer for meteoritic contributions to the surface materials. APXS data from the Mars Exploration Rovers are consistent with a 1% to 3% chondritic input to basaltic soils, Meridiani outcrop rocks, and Clovis class materials.

[71] 2. Nickel is a geochemically mobile element at the Martian surface, concentrating in hematite-rich spherules at Meridiani through aqueous processes. Nickel mobility in solution may also be partially responsible for the enhanced concentrations in Clovis class rocks of the Columbia Hills.

[72] 3. Nearly all Martian dust is attracted to magnets, possibly resulting from the presence of high-susceptibility np-Ox and small quantities of titanomagnetite in each grain. A portion of the titanomagnetite may have formed through meteoritic processes, involving the recondensation of material vaporized or melted during impact or atmospheric entry.

[73] 4. On the basis of the inferred quantity of meteoritic Ni and assuming a chondritic composition for the influx, a quantity of carbon equivalent to an average of 300 to 1000 ppm should have been delivered to the upper few meters of the Martian regolith. Some of the carbon-containing compounds could have pyrolyzed to carbon dioxide during entry. The remainder may have oxidized due to exposure to the Martian surface environment, or might still be present but not yet detected in the surface or subsurface.

[74] **Acknowledgments.** We thank the members of the MER project who enable daily science observations at the Spirit and Opportunity landing sites, K. Herkenhoff and M. Rosiek for the processed Microscopic Imager images, T. Myrick for discussions on the RAT, and H. Newsom and Y. Langevin for thoughtful and constructive reviews. R.V.M., D.W.M., and D.W.M. acknowledge support of the NASA Mars Exploration Rover Project and the NASA Johnson Space Center. The APXS was funded by the Max Planck Society and by the German Space Agency (DLR). R.G. acknowledges support from the University of Guelph and the Canadian Space Agency. A portion of the work described in this paper was conducted at the Jet Propulsion Laboratory, California Institute of Technology, under a contract with the National Aeronautics and Space Administration.

References

Adolfsson, L. G., B. A. S. Gustafson, and C. D. Murray (1996), The Martian atmosphere as a meteoroid detector, *Icarus*, *119*, 144–152.

Arlauckas, S. A., S. M. McLennan, and D. H. Lindsley (2006), The effect of low-temperature acidic weathering on the magnetic signature of primary Fe-Ti oxides on Mars, *Lunar Planet. Sci.*, *XXXVII*, 1609.

Bada, J. L., et al. (2005), New strategies to detect life on Mars, *Astron. Geophys.*, *46*, 6.26–6.27, doi:10.1111/j.1468-4004.2005.46626.x.

Bartlett, P. W., B. Basso, A. Kusack, J. Wilson, and K. Zacny (2005), New rock physical properties assessments from the Mars Exploration Rover Rock Abrasion Tool (RAT), *Eos Trans. AGU*, *86*(52), Fall Meet. Suppl., P21A-0135.

Basaltic Volcanism Study Project (1981), *Basaltic Volcanism on the Terrestrial Planets*, 1286 pp., Elsevier, New York.

Bell, J. F., III, et al. (2003), Mars Exploration Rover Athena Panoramic Camera (Pancam) investigation, *J. Geophys. Res.*, *108*(E12), 8063, doi:10.1029/2003JE002070.

Benner, S. A., K. G. Devine, L. N. Matveeva, and D. H. Powell (2000), The missing organic molecules on Mars, *Proc. Natl. Acad. Sci. U. S. A.*, *97*, 2425–2430.

Bertelsen, P., et al. (2004), Magnetic Properties Experiments on the Mars exploration Rover Spirit at Gusev crater, *Science*, *305*, 827–829.

Beukes, J. P., E. W. Giesekke, and W. Elliott (2000), Nickel retention by goethite and hematite, *Miner. Eng.*, *13*, 1573–1579.

Biemann, K., et al. (1977), The search for organic substances and inorganic volatile compounds in the surface of Mars, *J. Geophys. Res.*, *82*, 4641–4658.

Bland, P. A. (2001), Quantification of meteorite infall rates from accumulations in deserts, and meteorite accumulations on Mars, in *Accretion of Extraterrestrial Matter Throughout Earth's History*, edited by B. Peucker-Ehrenbrink and B. Schmitz, pp. 267–303, Springer, New York.

Boslough, M. B. (1988), Evidence for meteoritic enrichment of the Martian regolith, *Lunar Planet. Sci.*, *XIX*, 120–121.

Boslough, M. B. (1991), Shock modification and chemistry of planetary geologic processes, *Annu. Rev. Earth Planet. Sci.*, *19*, 101–130.
Bradley, J. P., L. P. Keller, D. E. Brownlee, and K. L. Thomas (1996), Reflectance spectroscopy of interplanetary dust particles, *Meteorit. Planet. Sci.*, *31*, 394–402.
Carr, M. H. (1984), *The Surface of Mars*, 232 pp., Yale Univ. Press, New Haven, Conn.
Chou, C.-L., W. V. Boynton, R. W. Bild, J. Kimberlin, and J. T. Wasson (1976), Trace element evidence regarding a chondritic component in howardite meteorites, *Proc. Lunar Sci. Conf. 7th*, 3501–3518.
Christensen, P. R., et al. (2003), Miniature Thermal Emission Spectrometer for the Mars Exploration Rovers, *J. Geophys. Res.*, *108*(E12), 8064, doi:10.1029/2003JE002117.
Christou, A. A., and K. Beurle (1999), Meteoroid streams at Mars: Possibilities and implications, *Planet. Space Sci.*, *47*, 1475–1485.
Clark, B. C., and A. K. Baird (1979), Is the Martian lithosphere sulfur rich?, *J. Geophys. Res.*, *84*, 8395–8403.
Clark, B. C., and D. C. van Hart (1981), The salts of Mars, *Icarus*, *45*, 370–378.
Clark, B. C., et al. (2005), Chemistry and mineralogy of outcrops at Meridiani Planum, *Earth Planet. Sci. Lett.*, *240*, 73–94.
Coey, J. M. D., S. Morup, M. B. Madsen, and J. M. Knudsen (1990), Titanomaghemite in magnetic soils on Earth and Mars, *J. Geophys. Res.*, *95*, 14,423–14,425.
Davis, P. (1993), Meteoroid impacts as seismic sources on Mars, *Icarus*, *105*, 469–478.
Flynn, G. J. (1996), The delivery of organic matter from asteroids and comets to the early surface of Mars, *Earth Moon Planets*, *72*, 469–474.
Flynn, G. J., and D. S. McKay (1990), An assessment of the meteoritic contribution to the Martian soil, *J. Geophys. Res.*, *95*(B9), 14,497–14,509.
Gellert, R., et al. (2004), Chemistry of rocks and soils in Gusev crater from the alpha particle X-ray spectrometer, *Science*, *305*, 829–832.
Gellert, R., et al. (2006), Alpha Particle X-Ray Spectrometer (APXS): Results from Gusev crater and calibration report, *J. Geophys. Res.*, *111*, E02S05, doi:10.1029/2005JE002555.
Genge, M. J., and M. M. Grady (1998), Melted micrometeorites from Antarctic ice with evidence for the separation of immiscible Fe-Ni-S liquids during entry heating, *Meteorit. Planet. Sci.*, *33*, 425–434.
Goetz, W., et al. (2005), Indication of drier periods on Mars from the chemistry and mineralogy of atmospheric dust, *Nature*, *436*, 62–65.
Golombek, M. P., et al. (2006a), Erosion rates at the Mars Exploration Rover landing sites and long-term climate change on Mars, *J. Geophys. Res.*, *111*, E12S10, doi:10.1029/2006JE002754.
Golombek, M. P., et al. (2006b), Geology of the Gusev cratered plains from the Spirit rover transverse, *J. Geophys. Res.*, *111*, E02S07, doi:10.1029/2005JE002503.
Gorevan, S. P., et al. (2003), Rock Abrasion Tool: Mars Exploration Rover mission, *J. Geophys. Res.*, *108*(E12), 8068, doi:10.1029/2003JE002061.
Grant, J. A., et al. (2006), Crater gradation in Gusev crater and Meridiani Planum, Mars, *J. Geophys. Res.*, *111*, E02S08, doi:10.1029/2005JE002465.
Greeley, R., et al. (2006), Gusev crater: Wind-related features and processes observed by the Mars Exploration Rover Spirit, *J. Geophys. Res.*, *111*, E02S09, doi:10.1029/2005JE002491.
Grotzinger, J. P., et al. (2005), Stratigraphy and sedimentology of a dry to wet eolian depositional system, Burns formation, Meridiani Planum, Mars, *Earth Planet. Sci. Lett.*, *240*, 11–72.
Halliday, A. N., H. Wänke, J. L. Birck, and R. N. Clayton (2001), The accretion, composition and early differentiation of Mars, *Space Sci. Rev.*, *96*, 197–230.
Hargraves, R. B., D. W. Collinson, R. E. Arvidson, and C. R. Spitzer (1977), The Viking magnetic properties experiment: Primary mission results, *J. Geophys. Res.*, *82*, 4547–4558.
Hartmann, W. K. (2005), Martian cratering 8: Isochron refinement and the chronology of Mars, *Icarus*, *174*, 294–320.
Haskin, L. A., et al. (2005), Water alteration of rocks and soils on Mars at the Spirit rover site in Gusev crater, *Nature*, *436*, 66–69.
Herkenhoff, K. E., et al. (2003), Athena Microscopic Imager investigation, *J. Geophys. Res.*, *108*(E12), 8065, doi:10.1029/2003JE002076.
Hörz, F., M. J. Cintala, W. C. Rochelle, and B. Kirk (1999), Collisionally processed rocks on Mars, *Science*, *285*, 2105–2107.
Hunt, C. P., B. M. Moskowitz, and S. K. Banerjee (1995), Magnetic properties of rocks and minerals, in *Rock Physics and Phase Relations: A Handbook of Physical Constants*, *AGU Ref. Shelf*, vol. 3, edited by T. J. Ahrens, pp. 189–204, AGU, Washington, D. C.
Hurowitz, J. A., S. M. McLennan, N. J. Tosca, R. E. Arvidson, J. R. Michalski, D. W. Ming, C. Schröder, and S. W. Squyres (2006), In situ and experimental evidence for acidic weathering of rocks and soils on Mars, *J. Geophys. Res.*, *111*, E02S19, doi:10.1029/2005JE002515.
Hviid, S. F., et al. (1997), Magnetic properties experiments on the Mars Pathfinder lander: Preliminary results, *Science*, *278*, 1768–1770.
Klingelhöfer, G., et al. (2003), Athena MIMOS II Mössbauer spectrometer investigation, *J. Geophys. Res.*, *108*(E12), 8067, doi:10.1029/2003JE002138.
Lemmon, M. T., et al. (2004), Atmospheric imaging results from the Mars exploration rovers: Spirit and Opportunity, *Science*, *306*, 1753–1756.
Lodders, K. (1998), A survey of shergottite, nakhlite, and chassigny meteorities whole-rock compositions, *Meteorit. Planet. Sci.*, *33*, A183–A190.
Lodders, K. (2003), Solar system abundances and condensation temperatures of the elements, *Astrophys. J.*, *591*(2), 1220–1247.
Lodders, K., and B. Fegley (1998), Presolar silicon carbide grains and their parent stars, *Meteorit. Planet. Sci.*, *33*(4), 871–880.
Madsen, M. B., D. P. Agerkvist, H. P. Gunnlaugsson, S. F. Hviid, J. M. Knudsen, and L. Vistisen (1995), Titanium and the magnetic phase on Mars, *Hyperfine Interactions*, *95*, 291–394.
Madsen, M. B., et al. (2003), Magnetic Properties Experiments on the Mars Exploration Rover mission, *J. Geophys. Res.*, *108*(E12), 8069, doi:10.1029/2002JE002029.
Mahaffy, P. R., and the SAM Science Team (2005), Organics and isotopes analysis on the 2009 Mars Science Laboratory, paper presented at 37th DPS Meeting, Div. for Planet. Sci., Am. Astron. Soc., Cambridge, U. K.
Maki, J. N., et al. (2003), Mars Exploration Rover Engineering Cameras, *J. Geophys. Res.*, *108*(E12), 8071, doi:10.1029/2003JE002077.
Malin, M. C., et al. (2005), MOC View of Spirit's Trek to the Columbia Hills, NASA's Planetary Photojournal, *PIA07192*, NASA, Washington, D. C., 3 Jan. (Available at http://photojournal.jpl.nasa.gov/catalog/PIA07192)
McLennan, S. M., et al. (2005), Provenance and diagenesis of the evaporite-bearing Burns formation, Meridiani Planum, *Mars, Earth Planet. Sci. Lett.*, *240*, 95–121.
McSween, H. Y., et al. (2006a), Characterization and petrologic interpretation of olivine-rich basalts at Gusev Crater, Mars, *J. Geophys. Res.*, *111*, E02S10, doi:10.1029/2005JE002477.
McSween, H. Y., S. W. Ruff, R. V. Morris, J. F. Bell, K. E. Herkenhoff, R. Gellert, and the Athena Science Team (2006b), Backstay and Irvine: Alkaline volcanic rocks from Gusev Crater, Mars, *Lunar Planet. Sci.*, *XXXVII*, 1120.
Melosh, H. J. (1989), *Impact Cratering: A Geologic Process*, 245 pp., Oxford Univ. Press, New York.
Meyer, C. (2003), *Mars Meteorite Compendium—2003*, *NASA JSC #27672 Rev. B*, NASA, Washington, D. C.
Ming, D. W., et al. (2006), Geochemical and mineralogical indicators for aqueous processes in the Columbia Hills of Gusev crater, Mars, *J. Geophys. Res.*, *111*, E02S12, doi:10.1029/2005JE002560.
Mittlefehldt, D. W., F. Hörz, T. H. See, E. R. D. Scott, and S. A. Mertzman (2005), Geochemistry of target rocks, impact_melt particles and metallic spherules from Meteor Crater, Arizona: Empirical evidence on the impact process, in *Large Meteorite Impacts III*, edited by T. Kenkmann, F. Hörz, and A. Deutsch, *Spec. Pap. Geol. Soc. Am.*, *384*, 367–390.
Mittlefehldt, D. W., R. Gellert, T. McCoy, H. Y. McSween Jr., R. Li, and the Athena Science Team (2006), Possible Ni-rich mafic-ultramafic magmatic sequence in the Columbia Hills: Evidence from the Spirit rover, *Lunar Planet. Sci.*, *XXXVII*, 1505.
Morris, R. V., D. G. Agresti, H. V. Lauer Jr., J. A. Newcomb, T. D. Shelfer, and A. V. Murali (1989), Evidence for pigmentary hematite on Mars based on optical magnetic and Mossbauer studies of superparamagnetic (nanocrystalline) hematite, *J. Geophys. Res.*, *94*, 2760–2778.
Morris, R. V., J. J. Gooding, H. V. Lauer Jr., and R. B. Singer (1990), Origins of Marslike spectral and magnetic properties of a Hawaiian palagonitic soil, *J. Geophys. Res.*, *95*, 14,427–14,434.
Morris, R. V., et al. (2000), Mineralogy, composition, and alteration of Mars Pathfinder rocks and soils: Evidence from multispectral, elemental, and magnetic data on terrestrial analogue, SNC meteorite, and Pathfinder samples, *J. Geophys. Res.*, *105*, 1757–1817.
Morris, R. V., D. C. Golden, D. W. Ming, T. D. Shelfer, L. C. Jorgensen, J. F. Bell III, T. G. Graff, and S. A. Mertzman (2001a), Phyllosilicate-poor palagonitic dust form Mauna Kea Volcano (Hawaii): A mineralogical analogue for magnetic Martian dust?, *J. Geophys. Res.*, *106*, 5057–5083.
Morris, R. V., G. E. Lofgren, L. Le, and T. D. Shelfer (2001b), Crystallization of oxide and silicate phases from impact melts with average Martian soil composition, *Lunar Planet. Sci.*, *XXXII*, Abstract 2012.
Morris, R. V., et al. (2006a), Mössbauer mineralogy of rock, soil, and dust at Gusev crater, Mars: Spirit's journey through weakly altered olivine basalt on the plains and pervasively altered basalt in the Columbia Hills, *J. Geophys. Res.*, *111*, E02S13, doi:10.1029/2005JE002584.

Morris, R. V., et al. (2006b), Mössbauer mineralogy of rock, soil, and dust at Meridiani Planum, Mars: Opportunity's journey across sulfate-rich outcrop, basaltic sand and dust, and hematite lag deposits, *J. Geophys. Res.*, doi:10.1029/2005JE002791, in press.

Myrick, T. M., K. Davis, and J. Wilson (2004), Rock Abrasion Tool, paper presented at 37th Aerospace Mechanisms Symposium, NASA Johnson Space Center, Houston, Tex.

Newsom, H. E., and J. J. Hagerty (1997), Chemical components of the Martian soil: Melt degassing, hydrothermal alteration, and chondritic debris, *J. Geophys. Res.*, *102*(E8), 19,345–19,355.

Newsom, H. E., M. J. Nelson, C. K. Shearer, and D. S. Draper (2005), The Martian soil as a geochemical sink for hydrothermally altered crustal rocks and mobile elements: Implications of early MER results, *Lunar Planet Sci.* [CD-ROM], *XXXVI*, Abstract 1142.

Pesnell, W. D., and J. Grebowsky (2000), Meteoric magnesium ions in the Martian atmosphere, *J. Geophys. Res.*, *105*, 1695–1707.

Pierazzo, E., and H. J. Melosh (2000), Hydrocode modeling of oblique impacts: The fate of the projectile, *Meteorit. Planet. Sci.*, *35*, 117–130.

Pollack, J. B., D. S. Colburn, F. M. Flaser, R. Kahn, C. E. Carlston, and D. Pidek (1979), Properties and effects of dust particles suspended in the Martian atmosphere, *J. Geophys. Res.*, *84*, 2929–2945.

Rieder, R., R. Gellert, J. Brückner, G. Klingelhöfer, G. Dreibus, A. Yen, and S. W. Squyres (2003), The new Athena alpha particle X-ray spectrometer for the Mars Exploration Rovers, *J. Geophys. Res.*, *108*(E12), 8066, doi:10.1029/2003JE002150.

Rietmeijer, F. J. M. (1998), Interplanetary dust particles, in *Planetary Materials, Rev. Mineral.*, vol. 36, edited by J. J. Papike, p. 2-1–2-95, chap. 2, Mineral. Soc. of Am., Washington, D. C.

Rietmeijer, F. J. M. (2000), Interrelationships among meteoric metals, meteors, interplanetary dust, micrometeorites, and meteorites, *Meteorit. Plan. Sci.*, *35*, 1025–1041.

Rose, A. W., and G. C. Bianchimosquera (1993), Adsorption of Cu, Pb, Zn, Co, Ni, and Ag on goethite and hematite—A control on metal mobilization from red beds onto stratiform copper deposits, *Econ. Geol. Bull. Soc. Econ. Geol.*, *99*, 1226–1236.

Schröder, C., et al., (2006), A stony meteorite discovered by the Mars Exploration Rover Opportunity on Meridiani Planum, Mars, paper presented at 69th Annual Meeting of the Meteoritical Society, Zurich, Switzerland.

Selsis, F., M. T. Lemmon, J. Vaubaillon, and J. F. Bell III (2005), Extraterrestrial meteors: A Martian meteor and its parent comet, *Nature*, *435*, 581.

Soderblom, L. A., et al. (2004), Soils of Eagle Crater and Meridiani Planum at the Opportunity Rover Landing Site, *Science*, *306*, 1723–1726.

Squyres, S. W., and A. H. Knoll (2005), Sedimentary rocks at Meridiani Planum: Origin, diagenesis, and implications for life on Mars, *Earth Planet. Sci. Lett.*, *240*, 1–10.

Squyres, S. W., et al. (2006), Rocks of the Columbia Hills, *J. Geophys. Res.*, *111*, E02S11, doi:10.1029/2005JE002562.

Taylor, S. R. (1982), *Planetary Science: A Lunar Perspective*, 481 pp., Lunar and Planet. Inst., Houston, Tex.

Wänke, H. (1991), Chemistry, accretion, and evolution of Mars, *Space Sci. Rev.*, *56*, 1–8.

Wasson, J. T., W. V. Boynton, C. L. Chou, and P. A. Baedecker (1975), Compositional evidence regarding the influx of interplanetary materials onto the lunar surface, *Moon*, *13*, 121–141.

Wdowiak, T. J., L. P. Armendarez, D. G. Agresti, M. L. Wade, S. Y. Wdowiak, P. Claeys, and G. Izett (2001), Presence of an iron-rich nanophase material in the upper layer of the Cretaceous-Tertiary boundary clay, *Meteorit. Planet. Sci.*, *36*, 123–133.

Yen, A. S., and B. Murray (1998), The color of Mars: Oxidation of exogenic metallic iron, *Bull. Am. Astron. Soc.*, *30*(3), Abstract 22.02.

Yen, A. S., S. S. Kim, M. H. Hecht, M. S. Frant, and B. Murray (2000), Evidence that the reactivity of the Martian soil is due to superoxide ions, *Science*, *289*, 1909–1912.

Yen, A. S., et al. (2005), An integrated view of the chemistry and mineralogy of Martian soils, *Nature*, *436*, 49–54.

Zipfel, J., et al. (2004), APXS analyses of bounce rock—The first shergottite on Mars, *Meteorit. Planet. Sci.*, *39*, A118.

Zolensky, M. E., M. K. Weisberg, P. C. Buchanan, and D. W. Mittlefehldt (1996), Mineralogy of carbonaceous chondrite clasts in HED achondrites and the Moon, *Meteorit. Planet. Sci.*, *31*, 518–537.

J. F. Bell III and S. W. Squyres, Department of Astronomy, Cornell University, 428 Space Sciences Building, Ithaca, NY 14853, USA.

J. Brückner, Max Planck Institut für Chemie, Kosmochemie, D-55020 Mainz, Germany.

B. C. Clark, Lockheed Martin Corporation, Littleton, CO 80127, USA.

T. Economou, Enrico Fermi Institute, University of Chicago, Chicago, IL 60637, USA.

R. Gellert, Department of Physics, University of Guelph, Guelph, ON, Canada N1G 2W1.

M. Golombek and A. S. Yen, Jet Propulsion Laboratory, California Institute of Technology, Mail Code 183-501, 4800 Oak Grove Drive, Pasadena, CA 91109, USA. (albert.yen@jpl.nasa.gov)

B. L. Jolliff, Department of Earth and Planetary Sciences, Washington University, Campus Box 1169, One Brookings Drive, St. Louis, MO 63130, USA.

M. B. Madsen, Niels Bohr Institute, University of Copenhagen, DK-2100 Copenhagen, Denmark.

T. J. McCoy, National Museum of Natural History, Smithsonian Institution, MRC 119, Washington, DC 20560, USA.

S. M. McLennan, Department of Geosciences, State University of New York at Stony Brook, Stony Brook, NY 11794, USA.

H. Y. McSween Jr., Department of Earth and Planetary Sciences, University of Tennessee, Knoxville, TN 37996, USA.

D. W. Ming, D. W. Mittlefehldt, and R. V. Morris, NASA Johnson Space Center, Houston, TX 77058, USA.

C. Schröder, Johannes Gutenberg University, Mainz, Germany.

T. Wdowiak, Department of Physics, University of Alabama at Birmingham, Birmingham, AL 35294, USA.

J. Zipfel, Forschungsinstitut und Naturmuseum Senckenberg, Frankfurt, Germany.